DIVERSITY TECHNIQUES FOR ULTRAVIOLET COMMUNICATIONS

A Thesis

by

Maryam Haghighi Ardakani

Submitted to the
Graduate School of Sciences and Engineering
In Partial Fulfillment of the Requirements for
the Degree of

Master of Science

in the
Department of Electrical and Electronics Engineering

Özyeğin University
August 2016

Copyright © 2016 by Maryam Haghighi Ardakani

DIVERSITY TECHNIQUES FOR ULTRAVIOLET COMMUNICATIONS

Approved by:

Professor Murat Uysal, Advisor
Department of Electrical and Electronics Engineering
Özyeğin University

Professor Cenk Demiroglu
Department of Electrical and Electronics Engineering
Özyeğin University

Professor Gunes Karabulut Kurt
Faculty of Engineering
Istanbul Technical University

Date Approved: 17 August 2016

To my beloved husband, Alireza

and

to my dear parents

ABSTRACT

Strong molecular and aerosol scattering in ultraviolet (UV) wavelengths enable mechanisms where transmitter can communicate with the receiver in the absence of line of sight (LOS) link. Recent advances in solid state technologies have enabled the production of efficient semiconductor ultraviolet (UV) LED sources and detectors which led to a renewed interest in UV communication. Non-line-of-sight (NLOS) communication is particularly desirable to relax or eliminate pointing, acquisition and tracking requirements. This thesis investigates spatial diversity techniques for NLOS UV communication systems. Particularly, we explore cooperative diversity in the form of relaying and multi-input multi-output (MIMO) communications to extract spatial diversity advantages.

In the first chapter, we provide an overview of NLOS UV communication discussing its advantages and applications and present a literature survey. In the second chapter, we present the NLOS UV channel model used in this thesis.

In third chapter, we consider a cooperative UV system with orthogonal cooperation protocol and use DC biased optical orthogonal frequency division multiplexing (DCO-OFDM) as the underlying physical layer. Under the assumption that turbulence can be ignored, we study both amplify-and-forward (AF) and detect-and-forward (DF) relaying. We analyze BER performance of the cooperative OFDM UV system under consideration and optimize the performance through optimal power allocation. We also consider a variable-rate cooperative OFDM UV system and investigate bit loading (i.e., use of different modulation orders per subcarrier) in an effort to maximize the throughput.

In the fourth chapter, we further consider the effects of turbulence and investigate

the performance of a multi-hop UV system with DF relaying. Based on the asymptotic outage expressions, we present a diversity gain analysis and obtain the diversity order as a function of link distance and system parameters.

In fifth chapter, the performance of MIMO UV systems over turbulence channels is studied. We derive BER expressions for MIMO UV systems over NLOS log-normal turbulence channels. We also investigate the performance of single-input multiple-output (SIMO) and multiple-input single output (MISO) as special cases.

ÖZETÇE

Morötesi (ultraviolet UV) dalgaboyları vericinin alıcı ile doğrudan bir görüş hattı (line of sight LOS) olmadan haberleşebildiği mekanizmaları mümkün kılar. Katıhal teknolojilerindeki son ilerlemeler, yüksek verimli yarıiletken morötesi (UV) LED ışık kaynaklarının ve detektörlerin üretimine imkan tanımıştır ve bu da UV haberleşmesine olan ilginin artmasına yol açmıştır. Görüş hattı dışı (Non-line-of-sight - NLOS) haberleşme özellikle nişanlama ve takip gibi gereklilikleri ortadan kaldırdığı için tercih edilir. Bu tez, NLOS UV haberleşme sistemlerinde uzamsal çeşitleme tekniklerini incelemektedir. özellikle, uzamsal çeşitlemenin avantajlarını ortaya çıkarmak için, röle-destekli iletim ve çok-girişli çok çıkışlı (MIMO) haberleşme incelenmiştir.

Tezin birinci bölümüde, NLOS UV haberleşme, avantajları ve uygulamalarının tartışıldığı genel bir özet ve bir literatür araştırması sunulmuştur. İkinci bölümde ise bu tezde kullanılan NLOS UV kanal modeli ortaya konulmuştur.

Tezin üçüncü bölümünde, ortogonal işbirliği protokolü ile çalışan bir işbirlikli UV sistemi ele alınmış ve fiziksel katman olarak da doğru akım eklemeli optik ortogonal frekans bölmeli çoğullama (DCO-OFDM) kullanılmıştır. Türbülansın ihmal edilebileceği varsayımı altında, hem yükselt-ve-ilet (amplify-and-forward - AF) hem de çöz-ve-ilet (detect-and-forward DF) röleleme çalışılmıştır. İşbirlikli OFDM UV sisteminin bit hata oranı (bit error rate BER) başarımı incelenmiş ve terminaller arasında güç dağılım optimizasyonu yapılmıştır. Ayrıca değişken hızlı işbirlikli OFDM UV sistemi de ele alınmış ve veriyi maksimize etmek için bit yükleme (örneğin, her alt taşıyıcıda farklı kipleme derecelerinin kullanılması gibi) incelenmiştir.

Dördüncü bölümde, türbülansın etkileri ele alınmış ve DF röleli çok-atlamalı

UV sisteminin başarımı incelenmiştir. Asimptotik olarak çeşitleme kazancı analizi sunulmuş ve çeşitleme derecesi iletim mesafesine ve sistem parametrelerine bağlı olarak ifade edilmiştir.

Beşinci bölümde, MIMO UV sistemlerinin türbülans kanallarındaki başarımı çalışılmıştır. NLOS log-normal türbülans kanallarında MIMO UV sistemleri için BER ifadeleri elde edilmiştir. Ayrıca tek girişli çok çıkışlı (single-input multiple-output SIMO) ve çok girişli tek çıkışlı (multiple-input single-output MISO) gibi özel durumların da başarımı incelenmiştir.

ACKNOWLEDGEMENTS

All praises to Allah, the Almighty, for His showers of blessings throughout my studies to complete this thesis.

I would like to express my sincere gratitude to my supervisor Prof. Murat Uysal for the continuous support of my study and related research, for his patience, motivation, and immense knowledge. Furthermore I would like to thanks Prof. Refik Caglar Kizilirmak for his engagement through the learning process of this master thesis and support on the way.

Finally I thank my loved ones, my dear parents for their kindness and praying and my dear husband for his love, support and understanding which made the completion of this thesis possible.

TABLE OF CONTENTS

LIST OF TABLES

LIST OF FIGURES

CHAPTER I

INTRODUCTION

Optical wireless communication (OWC), refers to optical transmission in unguided media through the use of infrared (IR), visible (VL) or ultraviolet (UV) wavelengths. There is already a well-established literature on OWC systems that operate in IR and VL bands [1, 2]. On some occasions of OWC, the transmission may be blocked by an obstacle between the transmitter and the receiver. The solution is to utilize the non-line-of-sight (NLOS) optical scattering communication [3], where the transmitting direction and the receiving direction are not required to be perfectly aligned. Strong molecular and aerosol scattering in UV wavelengths enable the NLOS OWC [3, 4].

In this chapter, we provide an overview of NLOS UV communication highlighting its advantages and application areas. Then, we present a literature survey motivating the current work which focuses on spatial diversity techniques.

1.1 NLOS UV Communication

UV region in electromagnetic spectrum is divided to three sub bands: UV-A (315-400 nm), UV-B (280-315 nm) and UV-C (100-280 nm). The interest in optical communications at ultraviolet wavelengths is focused on the C portion of the ultraviolet spectrum [5]. The UV-C is solar blind at the ground level since large fraction of the UV from the sun in this band is filtered by the ozone layer in upper atmosphere. Hence, the effect of background noise is negligible. As a result, wide field-of-view (FOV) receivers can be deployed that significantly increase the received energy with little additional background noise; this is not the case, for example, with IR. Furthermore when UV waves traverse the atmosphere there is high degree of relatively angle-independent scattering. This creates diverse communication path from source

to destination and enables NLOS as well as LOS communication.

NLOS links are particularly desirable to relax or eliminate pointing, acquisition and tracking (PAT) requirements of conventional IR transmission. NLOS UV can be used as an alternative to outdoor IR links or in combination with existing optical and radio frequency (RF) links [3]. In areas where cellular and other forms of commercial communication infrastructure are either unavailable or unreliable, NLOS UV communication can serve as redundant links. For example, in an unattended ground sensor network NLOS UV communication can serve as either the primary means of communication between sensing nodes, or as a low-power paging system employed to activate higher-power communication and sensing systems.

Besides the advantages of NLOS UV transmission there are some limiting factors. For example, UV applications must be tempered by eye and skin exposure limits. The International Commission on NonIonizing Radiation Protection (ICNIRP) [6] and the International Electrotechnical Commission (IEC) regulate these limits.

Studies on UV channel modeling demonstrate that UV channel is of multipath nature due to the atmospheric scattering and large scattering volume which result in inter symbol interference (ISI). In addition NLOS UV links suffer large path loss due to underlying atmospheric scattering process. Furthermore, as the link range increases, turbulence induced fading potentially becomes another degrading factor.

1.2 Literature Review

NLOS UV communication has been investigated in various theoretical and experimental works. In this section we review some different communication techniques applied to NLOS UV transmission in the current literature.

1.2.1 Relay Assisted Transmission

One effective solution to deal with path loss and enable longer transmission ranges is relay-assisted transmission which has been earlier studied in the context of OWC

at IR and VL bands [7, 8]. The concept of relay-assisted communication was recently explored also at UV bands [9–13]. In [9], He et al investigate the bit error rate (BER) of an NLOS UV serial relaying (i.e., multi-hop) system, where nodes are located at equidistant from each other and demonstrate power saving advantages over direct transmission. In [10], Vavoulas et al consider a UV network in which nodes are independently distributed according to homogeneous Poison Point Process (PPP) in a service area and analyze the trade-off between node density and the degree of connectivity against other network parameters (i.e., transmit power, data rate, and error probability). In [11], an analytical expression for the node isolation probability in a serial multi-hop UV network is presented. In [12] Gong and Xu proposed a count and forward relay scheme for the optical wireless relay communication system and formulate the relay forwarding power optimization problem that minimizes the destination detection error probability given the relay forwarding power budget. In [13], Li et al focus on upper layer issues and propose protocols for neighbor discovery in an ad-hoc UV network.

It is worth mentioning that the main underlying assumption in most existing relay-assisted UV works is the assumption of non-dispersive (frequency-flat) channel and negligible atmospheric turbulence.

1.2.2 MIMO Transmission

Relay-assisted systems can be considered as a distributed spatial diversity system. The employment of co-located multiple transmitters/receivers can also improve link reliability (through diversity gain) or throughput rate (through multiplexing gain). Such systems have been well studied in wireless (radio-frequency) literature and also applied to OWC systems in IR wavelengths [14, 15]. The number of works which address the deployment of multiple transmitters and receivers in UV communication systems is rather limited [16–19]. In [16], a diversity receiver based on imaging optics

and a focal-plane detector array is proposed and it is shown that the proposed single-input multiple-output (SIMO) system achieves improvement in information rate over SISO counterparts. In [17], the bit error rate (BER) performance of a SIMO UV communication system with equal gain combining (EGC) is investigated under the assumption of path loss and background radiation effects. The work in [18] considers the use of two photomultiplier tube (PMT) receivers and investigates the BER performance. In [19], the performances of different equalizers such as maximum aposteriori probability (MAP) and maximum likelihood sequence estimation (MLSE) are investigated over frequency selective multi-input multi-output (MIMO) UV channels. In the aforementioned works [16–19], the effects of turbulence are neglected and only path loss is taken into account. The BER performance of SIMO NLOS UV systems in the presence of turbulence is studied in [20]. However, no closed form expression is provided. Furthermore, it is assumed that all receivers point out at the same common atmospheric volume which might not hold in practice.

1.2.3 Inter Symbol Interference Mitigation

There exist some works on point-to-point UV links [18–22] which further take into account the effect of frequency selectivity. In [18] spectral encoding is proposed and the maximum achievable data rates for different distances over a frequency-selective UV channel is calculated. In [19], different time-domain equalizers are employed to mitigate ISI in a MIMO UV communication system and present the BER performance through simulations. In [21], the capacity of a multipath UV channel is derived and error control coding mechanisms to approach the capacity is investigated.

Time-domain equalization becomes prohibitively complex for long channel impulse responses (CIRs) and/or for higher order modulation schemes. An efficient approach to mitigate ISI is orthogonal frequency division multiplexing (OFDM) which is a multi-carrier transmission system where the high-rate data stream is demultiplexed

and transmitted over a number of frequency subcarriers. An initial work on asymmetrically clipped optical (ACO) OFDM based UV communication is presented in [22] for point-to-point (direct) transmission.

1.3 Thesis Structure and Contributions

This thesis is organized as follows: In Chapter 2, we describe the NLOS channel impulse response and path loss modeling. Furthermore we review the literature on turbulence modeling and propose a closed form expression for NLOS turbulence induced fading in weak atmospheric turbulence conditions.

In Chapter 3, we propose the powerful combination of relay-assisted transmission and multi-carrier architecture based on OFDM. Specifically, we consider a cooperative diversity system with orthogonal cooperation protocol and use DC-biased optical OFDM (DCO-OFDM) as the underlying physical layer. We consider both amplify-and-forward (AF) and detect-and-forward (DF) relaying. We investigate the error rate performance of the proposed relay-assisted OFDM UV system under consideration and demonstrate performance gains over point-to-point OFDM UV systems. We further determine optimal power allocation (OPA) schemes to improve the performance. We also consider a variable-rate UV OFDM system and improve system throughput via bit loading.

In Chapter 4, we consider a multi-hop UV system with DF relaying and analyze its performance in the presence of lognormal atmospheric turbulence. We obtain the outage probability of the multi-hop UV system and quantify diversity gain as a function of system and channel parameters. We also present numerical results to confirm the accuracy of our derivations and discuss the effect of several system parameters on the outage probability and diversity gain.

In Chapter 5, we derive BER expressions for MIMO UV systems over NLOS log-normal turbulence channels. We also investigate the performance of single-input

multiple-output (SIMO) and multiple-input single output (MISO) as special cases. Simulation results are further provided to confirm the analytical findings.

Finally in Chapter 6, we present the conclusions of our works.

CHAPTER II

NLOS UV CHANNEL MODELING

2.1 Introduction

In this chapter, we first describe the NLOS link configuration and provide the channel impulse response used in our works. Furthermore we review the literature on NLOS turbulence modeling and propose a closed form expression for NLOS turbulence induced fading distribution in weak atmospheric turbulence condition.

2.2 NLOS UV Channel Impulse Response

The NLOS UV link configuration is illustrated in Fig.1. In this figure, d is the separation distance between transmitter and receiver, V denotes the common volume, and β_{TX} and β_{RX} are, respectively, transmitter and receiver elevation angles. θ_{TX} represents the beam divergence of transmitter and θ_{RX} is the receiver FOV. Let δV denote the differential volume. d_1 is the distance between the transmitter and δVwhile d_2 is the distance between the receiver and δV.

In the literature, analytical [23, 24], experimental [25] and simulation [26, 27] approaches have been used to determine the NLOS UV channel impulse response (CIR). Here, we adopt the analytical UV channel model in [23] where only single scatter propagation is considered and the scattered irradiance is calculated in an integral form. Let $k_s = k_s^{Ray} + k_s^{Mie}$ denote the atmospheric scattering coefficient where k_s^{Ray} and k_s^{Mie} are respectively due to molecular (Rayleigh) and aerosol (Mie) scattering. The calculation of irradiance is carried out in the prolate spheroidal coordinate. In this coordinate space, each point is uniquely determined with a radial component ξ, an angular coordinate η and an azimuthal coordinate ϕ. The curves of constant

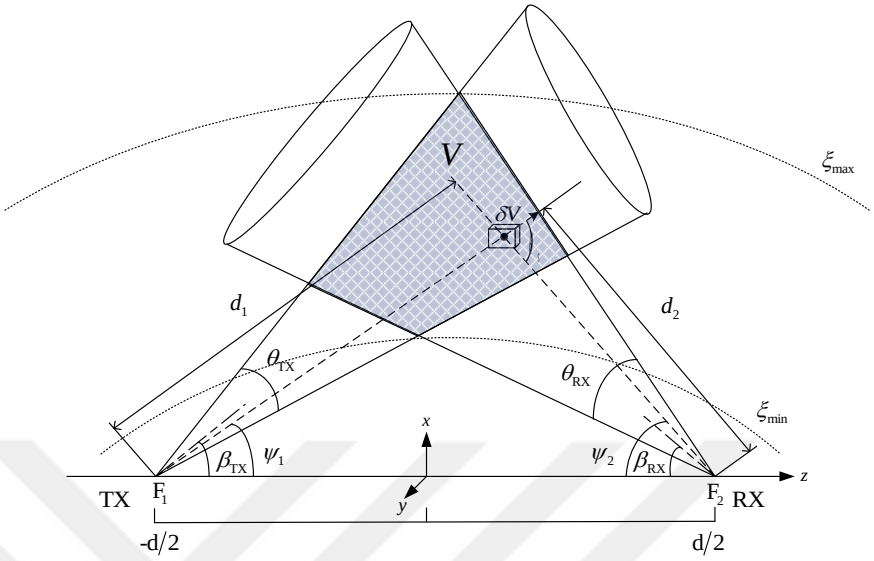

Figure 1: NLOS UV link between a transmitter and a receiver.

$\xi = (d_1 + d_2)\,/d$ are prolate spheroids and takes values larger than 1. Prolate spheroid surface is basically a surface generated by the rotation of an ellipse about its major axis. The curves of constant $\eta = (d_1 - d_2)\,/\,d$ are hyperboloids of revolution and takes values in the range of $[-1,\ 1]$. The azimuthal angle is the angle measured from the x-axis to the orthogonal projection of a point of spherical coordinates in the xy-plane of xyz-space.

Assume that an impulse with optical power I_t is emitted from the transmitter at $t = 0$. Then the energy scattered from the differential volume δVat the receiver is [23]

$$\frac{I_t A_{\mathrm{RX}} k_s \cos(\zeta) \exp\left[-k_e\,(d_1 + d_2)\right]}{4\pi\Omega_T\,(d_1 d_2)^2}\,\Psi(\theta_s)\,\delta V, \tag{1}$$

where $\Omega_T = 4\pi \sin^2(\theta_{\mathrm{TX}}/4)$ is the solid cone angle of the transmitter cone, and A_{R} and k_e respectively denote receiver area and atmospheric extinction coefficient. ζ is the angle between the receiver axis and a vector pointing from the receiver to the volume element.

In (1), $\Psi(\theta_s)$ is the single scatter phase function and can be modeled as a weighted

sum of Rayleigh and Mie scattering phase functions given by [26]

$$\Psi\left(\theta_s\right) = \frac{k_s^{Ray}}{k_s}\Psi^{Ray}\left(\theta_s\right) + \frac{k_s^{Mie}}{k_s}\Psi^{Mie}\left(\theta_s\right). \tag{2}$$

Here, $\Psi^{Ray}\left(\theta_s\right)$ and $\Psi^{Mie}\left(\theta_s\right)$ are defined as

$$\Psi^{Ray}\left(\theta_s\right) = \frac{3}{4\left(1+2c_1\right)}\left[1+3c_1+\left(1-c_1\right)\left(\cos\left(\theta_s\right)\right)^2\right], \tag{2.a}$$

$$\Psi^{Mie}\left(\theta_s\right) = \frac{1-c_2^2}{\left(1+c_2^2-2c_2\cos\left(\theta_s\right)\right)^{3/2}} + \frac{0.5c_3\left(3\left(\cos\left(\theta_s\right)\right)^2-1\right)\left(1-c_2^2\right)}{\left(1+c_2^2\right)^{3/2}}, \tag{2.b}$$

where $c_1 = 0.017$, $c_2 = 0.72$ and $c_3 = 0.5$ [26].

Transmitter and receiver are respectively located on points F_1 and F_2 which are the focal points of the ellipse so d becomes the interfocal distance. A property of prolate spheroidal coordinate is that the sum of distances from two focis to any point on the spheroid surface is constant for a given ξ, $\xi_{\min} \le \xi \le \xi_{\max}$. Energy scattered from the surface ξ takes duration of $t = (d_1 + d_2)/\,c$ to arrive at the receiver where c is the speed of light. Hence the relationship between ξ and t can be represented as $\xi = ct/\,.d$; this means that each ξ corresponds to a particular time delay. Considering (1) and following the steps in [23] the optical power delay profile,$C\left(t\right)$, for the interval of $t_{\min} \le t \le t_{\max}$ (corresponding to $\xi_{\min} \le \xi \le \xi_{\max}$) is obtained as [23]

$$C(t) = \frac{I_t c k_s A_{\mathrm{RX}} \exp(-k_e c t)}{2\pi\Omega_T d^2}\int_{\eta_1(t)}^{\eta_2(t)} \frac{2g\left(\phi(t,\eta)\right)\Psi(\theta_s)}{\left(ct/\,.d\right)^2-\eta^2}d\eta, \quad t_{\min} \le t \le t_{\max}, \tag{3}$$

where $g\left(\phi(t,\eta)\right) = \phi(t,\eta)\cos\beta_{RX}\cos\psi_1 + \sin\beta_{RX}\sin\psi_1\sin\phi(t,\eta)$. The value of $\phi(t,\eta)$ and limits of the integral, i.e., $\eta_1(t)$ and $\eta_2(t)$, are dictated by the common volume between transmitter and receiver [23].

In order to measure the amount of attenuation due to scattering in channel we have

$$\ell^s = \frac{1}{I_t}\int_{t_{\min}}^{t_{\max}} C\left(t\right)dt. \tag{4}$$

For the time dispersion, the rms (root mean square) delay spread of optical power delay profile,$C(t)$, is defined as

$$\tau_d = \left[\frac{\int (t-\bar{t})^2 C(t)\, dt}{\int C(t)\, dt} \right]^{1/2}, \tag{5}$$

where $\bar{t}$ is the mean delay. Let B_s denote the data rate. A channel is classified as "frequency-selective" for $B_s\tau_d \geq 1$. If $B_s\tau_d \ll 1$, then it is classified as "frequency-flat" channel.

The energy scattered from the differential volume δV in V at the receiver is given by (1). In order to obtain the overall energy scattered from V ones need to perform integration. To obtain tractable analytical results and gain some insight into the link behavior, [28] assumes the common volume is small enough such that we can approximate $\zeta = 0$ and simplify the integration. Furthermore to obtain the volume of V the transmitter beam is considered small enough such that V can be approximated by a frustum of the right cone. In such case the volume is expressed as $V = (\pi/3)(D_1^2 h_1 - D_2^2 h_2)$ where $h_1 = d_1 + d_2\theta_{\mathrm{RX}}/2$ and $D_1 = h_1\theta_{\mathrm{TX}}/.2$ are respectively the height and the radius of the bottom surface of the larger cone. Similarly, we have $h_2 = d_1 - d_2\theta_{\mathrm{RX}}/.2$ and $D_2 = h_2\theta_{\mathrm{TX}}/2$ for the smaller cone [28]. Also we have $\theta_s = \beta_{\mathrm{TX}} + \beta_{\mathrm{RX}}$. Finally by considering the approximations in [28] the attenuation due to scattering can be written as

$$\ell^s \approx \frac{A_{\mathrm{RX}} k_s \exp\left[-k_e (d_1+d_2)\right] \Psi(\theta_s)\, V}{4\pi\Omega_T (d_1 d_2)^2}. \tag{6}$$

2.3 NLOS Turbulence Induced Fading

In the existing literature on UV communication, it is commonly assumed that turbulence induced fading can be ignored by restricting the communication range within hundreds of meters and considering clear weather conditions. It is however well known that inhomogeneities in the temperature and the pressure of the atmosphere result in variations of the refractive index. This causes atmospheric turbulence and manifests

itself as random fluctuations in the received signal. There are some sporadic works on NLOS turbulence modeling [29–31]. In [29], Hutt and Tofsted have experimentally shown that the received density distribution of LOS UV radiation follows log-normal (lnN) distribution in the case of weak turbulence similar to LOS links operating at infrared frequencies. In [30], Ding et al. worked on statistical turbulence modelling for a NLOS UV link. They considered NLOS UV link as a combination of two LOS paths, one from transmitter to the common volume and another from the common volume to the receiver. The marginal probability density function (PDF) of the received optical power at the receiver side of the NLOS link can be obtained by integrating over the joint distribution of these two LOS paths. The work in [30] does not provide a closed-form for this integration, but numerically shows that the resulting model fits to the log-normal distribution. In the following, we derive a closed form expression for this.

Similar to [28], transmitter beam is considered small enough such that Vcan be approximated by a frustum of the right cone. Furthermore the fading within the Vcan be considered constant for a fixed geometry [30]. The optical received power at V in the absence of turbulence is given by

$$I_{v_0} = \frac{I_t k_s \exp\left[-k_e d_1\right] \Psi\left(\theta_s\right) V}{\Omega_T d_1^2}. \tag{7}$$

Let I_v and I_r respectively denote the received optical powers in V and at the receiver in the presence of the turbulence. The PDF for I_v and the conditional PDF for I_r are respectively expressed by [30]

$$f\left(I_v\right) = \frac{1}{\sqrt{2\pi}\sigma_{d_1} I_v} \exp\left(-\frac{1}{2\sigma_{d_1}^2}\left(\ln\left(\frac{I_v}{I_{v_0}}\right) + \mu_1\right)^2\right), \tag{8}$$

$$f\left(I_r|I_v\right) = \frac{1}{\sqrt{2\pi}\sigma_{d_2} I_r} \exp\left(-\frac{1}{2\sigma_{d_2}^2}\left(\ln\left(\frac{I_r}{E\left[I_r|I_v\right]}\right) + \mu_2\right)^2\right), \tag{9}$$

with $\mu_i = 0.5\sigma_{d_i}^2 + a_{d_i}\ln 10/\ .10$ where $a_{d_i} = 2\sqrt{23.17 C_n^2 k^{7/6} d_i^{11/6}}$ and $\sigma_{d_i}^2 \cong 1.23 C_n^2 k^{7/6} d_i^{11/6}$. Here, $k = 2\pi/\lambda$ is the wave number, λ is wavelength and C_n^2 stands for refractive index structure coefficient and $E[\cdot]$ is the expectation operation. In (9), $E[I_r|I_v]$ is given by

$$E[I_r|I_v] = \frac{I_v A_{\mathrm{RX}} \exp(-k_e d_2)}{4\pi d_2^2}. \tag{10}$$

The joint PDF of I_v and I_r is $f(I_r, I_v) = f(I_r|I_v) f(I_v)$. Replacing (8) and (9) therein and following the derivation steps in the Appendix I, we obtain the closed-form PDF of received optical power as [31]

$$f(I_r) = \frac{1}{\sqrt{2\pi}\sigma_{NLOS} I_r} exp\left(-\frac{1}{2\sigma_{NLOS}^2}\left(ln\left(\frac{I_r}{I_0^{NLOS}}\right) + \mu_{NLOS}\right)^2\right), \tag{11}$$

where $\sigma_{NLOS}^2 = \sigma_{d_1}^2 + \sigma_{d_2}^2$, $\mu_{NLOS} = \mu_1 + \mu_2$ and I_0^{NLOS} is given by

$$I_0^{NLOS} = \frac{I_t k_s \Psi(\theta_s) A_{\mathrm{RX}} \exp(-k_e (d_{1+} d_2)) V}{\Omega_T 4\pi d_2^2 d_1^2}. \tag{12}$$

It is worth noting that I_0^{NLOS} corresponds to the received power at receiver in the absence of turbulence under single scattering assumption [28].

In the following, we also compare (11) with the PDF of a LOS UV link for the same distance given by

$$f(I_r) = \frac{1}{\sqrt{2\pi}\sigma_{LOS} I_r} exp\left(-\frac{1}{2\sigma_{LOS}^2}\left(\ln\left(\frac{I_r}{I_0^{LOS}}\right) + \mu_{LOS}\right)^2\right). \tag{13}$$

In (13), we have $\sigma_{LOS}^2 = 1.23 C_n^2 k^{7/6} d^{11/6}$, $\mu_{LOS} = 0.5\sigma_{LOS}^2 + a_d \ln 10/10$ and I_0^{LOS} is given by

$$I_0^{LOS} = \frac{I_t A_{\mathrm{RX}} exp(-k_e d)}{4\pi d^2}. \tag{14}$$

Using $d_1 = d\sin(\beta_{RX}) / \sin(\theta_S)$ and $d_2 = d\sin(\beta_{TX}) / \sin(\theta_S)$, we can write σ_{NLOS}^2 as

$$\sigma_{NLOS}^2 = 1.23 C_n^2 k^{7/6} d^{\frac{11}{6}} \frac{\sin(\beta_{\mathrm{RX}})^{\frac{11}{6}} + \sin(\beta_{\mathrm{TX}})^{\frac{11}{6}}}{\sin(\theta_s)^{\frac{11}{6}}}. \tag{15}$$

Therefore, $\sigma^2_{NLOS} = \Lambda\sigma^2_{LOS}$ where $\Lambda = \left(\sin(\beta_{\rm RX})^{11/6} + \sin(\beta_{\rm TX})^{11/6}\right) \Big/ \sin(\theta_s)^{11/6}$. For $\Lambda < 1$ (which can be satisfied with the proper choice of small elevation angles), it is interesting to note that NLOS transmission experiences less fluctuation due to turbulence in comparison to LOS transmission.

For the numerical study in this section, we assume $(\theta_{\rm TX}, \beta_{\rm TX},\ \theta_{\rm RX}, \beta_{\rm RX}) = (8\text{mrd},\ 30^\circ,\ 45^\circ,\ 30^\circ)$, $k_s^{Ray} = 0.266\ \text{km}^{-1}$, $k_s^{Mie} = 0.284\ \text{km}^{-1}$, $k_e = 1.352\ \text{km}^{-1}$, $\lambda = 260$ nm, and $A_{\rm RX} = 1.77\ \text{cm}^2$ unless otherwise specified.

In Figs 2 and 3 we illustrate the PDF of instantaneous received optical power in NLOS link given by (11) and compare it with the PDF of LOS link given by (13). The bird-fly distance between receiver and transmitter in both links is the same. We assume$C_n^2 = 10^{-15}\ \text{m}^{-2/3}$. It can be seen that by increasing d, the received instantaneous optical power variance increases. It is observed that for this geometry turbulence variance for LOS link is larger than that of NLOS link. However, the attenuation due to turbulence is less significant in comparison to NLOS link. It is also observed that even for small distances the fluctuation and attenuation due to turbulence may also introduces degradation to the system performance.

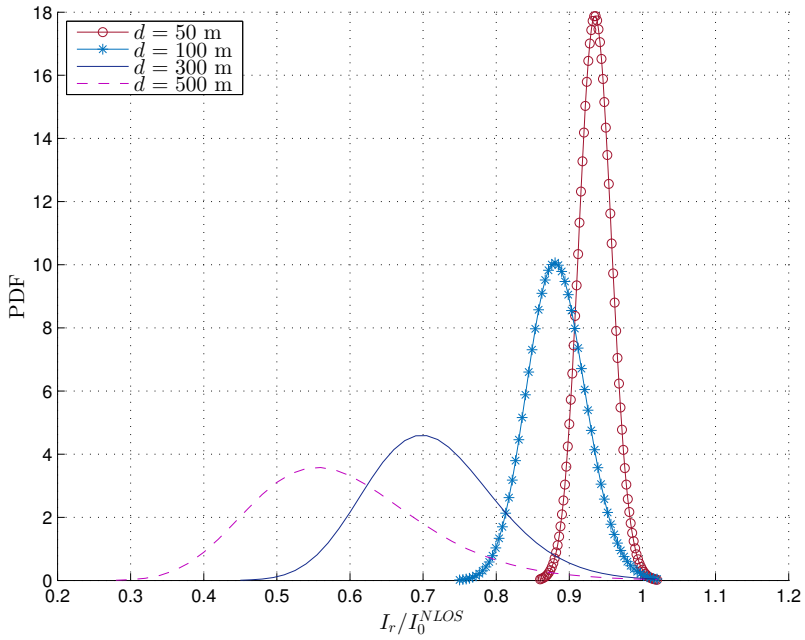

Figure 2: PDF of normalized instantaneous received optical powers for NLOS link.

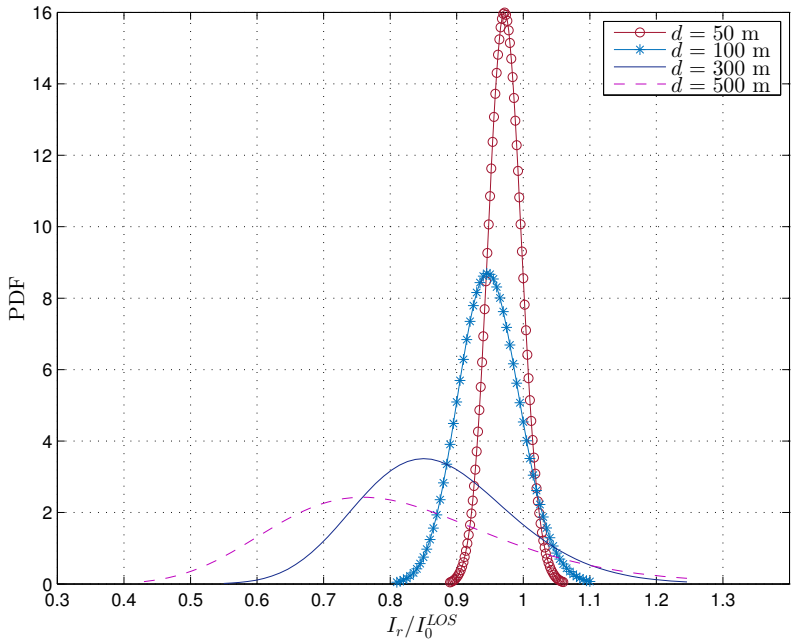

Figure 3: PDF of normalized instantaneous received optical powers for LOS link.

CHAPTER III

RELAY-ASSISTED OFDM FOR ULTRAVIOLET COMMUNICATIONS

3.1 Introduction

Relay-assisted transmission and OFDM are powerful tools to mitigate large path loss and ISI respectively. To the best of our knowledge, the powerful combination of relay-assisted transmission with OFDM architecture was not yet studied in the UV communication literature. To address this research gap, we propose the use of OFDM for a relay-assisted (cooperative) UV communication system in this chapter. Specifically, we consider a cooperative UV system with orthogonal cooperation protocol and use DCO-OFDM as the underlying physical layer. We study both AF and DF relaying. We analyze BER performance of the cooperative OFDM UV system under consideration and optimize the performance through optimal power allocation. We also consider a variable-rate cooperative OFDM UV system and investigate bit loading (i.e., use of different modulation orders per subcarrier) in an effort to maximize the throughput.

Notations: $*$ and $\otimes$ denotes convolution operation and circular convolution operation respectively. $Q(\cdot)$ is the tail probability of standard normal distribution. A $\rightarrow$ B denotes the link between node A and node B. $x(n) = .x(t)|_{t=nT_s}$ is the discretized version of continuous time domain signal $x(t)$. $x(n) \overset{\text{FFT}}{\leftrightarrow} X(i)$ represents the FFT transform pair, i.e., $X(i) = \sum_{n=0}^{N-1} x(n)e^{-j2\pi ni/N}$, $i = 0, 1, ...N-1$ are FFT coefficients for $x(n)$, $n = 0, 1, ...N-1$. Upper case bold face letters denote vectors. $X = [X(0), X(1) ....X(N-1)]$ where $X(i)$ denotes the i^{th} element of vector X.

3.2 Channel and System Model

3.2.1 Channel Model

We use the channel model presented section 2 of Chapter 2. We ignore the effects of turbulence assuming short transmission range and clear weather condition. As earlier discussed, the UV channel is of multipath nature in genereal. A channel is classified as frequency-selective for $B_s\tau_d \geq 1$ where τ_d is the channel delay spread and $B_s = 1/T_s$ is the data rate. In Table 1, we present the rms delay spreads for a set of system parameters under consideration. Our calculations yield that for data rates higher than 1.22 Mbits/sec, the channel is classified as frequency-selective for the configurations under consideration. There are several UV works which consider data rates of a few Mbits/sec [16, 18, 19, 21]. With the recent advancements in UV semiconductor technology, the data rates of UV communication systems will further increase. Therefore, frequency-selectivity is justified for practical purposes. In this section, we consider $B_s = 2$ Mbits/sec ($T_s = 0.5$ μsec) that satisfies the assumption of frequency-selectivity.

Table 1: Delay spread for different configurations under consideration.

Configuration	$(\beta_{\mathrm{TX}}, \beta_{\mathrm{RX}}, \theta_{\mathrm{TX}}, \theta_{\mathrm{RX}}, d)$	τ_d (μs)	$1/\tau_d$ ($\times 10^{-6}$)
1	$(90°, 90°, 20°, 30°, 100$ m$)$	1.51	0.66
2	$(90°, 80°, 20°, 30°, 40$ m$)$	0.82	1.22
3	$(80°, 90°, 20°, 30°, 60$ m$)$	0.99	1.01
4	$(90°, 90°, 20°, 40°, 100$ m$)$	1.33	0.75

Let $p(t)$ denote the impulse response of the pulse shaping filter. Considering a matched filter at the receiver side, the composite channel impulse response (CIR) for A $\rightarrow$ B link can be written as $h_{\mathrm{AB}}(t) = p(t) * C_{\mathrm{AB}}(t) * p(-t)$. We can further define the normalized CIR with unit energy as $\hat{h}_{\mathrm{AB}}(t) = h_{\mathrm{AB}}(t) \Big/ \sqrt{\int_{-\infty}^{+\infty} |h_{\mathrm{AB}}(t)|^2}$.

3.2.2 System Model

We consider a three node communication scenario with orthogonal cooperation (see Fig.4). Each node is equipped with one transmitter and one receiver and operates in half duplex mode. In Fig. 4, $\theta_{\mathrm{TX}}^{\mathrm{S}}$ and $\theta_{\mathrm{TX}}^{\mathrm{R}}$ are the transmitter beam divergences of source and relay, respectively. $\theta_{\mathrm{RX}}^{\mathrm{R}}$ and $\theta_{\mathrm{RX}}^{\mathrm{D}}$ are receiver FOVs of relay and destination, respectively. $\beta_{\mathrm{TX}}^{\mathrm{S}}$, $\beta_{\mathrm{RX}}^{\mathrm{R}}$, $\beta_{\mathrm{TX}}^{\mathrm{R}}$ and $\beta_{\mathrm{RX}}^{\mathrm{D}}$, respectively, denote source transmitter elevation angle, relay receiver elevation angle, relay transmitter elevation angle and destination receiver elevation angle. The relay node is located at an arbitrary position in the same two dimensional plane with source and destination nodes. In Fig.4, h denotes the orthogonal distance from relay node to the direct line connecting source and destination. In configurations under consideration, we assume source transmitter and destination receiver cones' axis are in the same plane and their projections lie on S-D line. On the other hand, the cones' axis projections of relay receiver and transmitter lie on S-R line and R-D line respectively. In the first transmission phase (i.e., broadcasting phase), the source node (S) transmits the signal which is heard by both relay I and destination (D) nodes, see common volumes labeled with V_{SD} and V_{SR}. In the second transmission phase (i.e., relaying phase), the source node remains silent and the relay transmits its signal to the destination via the common volume labeled as V_{RD}. Maximal Ratio Combining (MRC) is performed by destination to combine the received signals over two phases.

The block diagrams of source, relay and destination nodes are illustrated in Fig.5. At the source node, the input bit stream is first mapped to the modulation symbols s_1, s_2, ..., $s_{N/2-1}$, where N is the number of subcarriers. We assume M-QAM (quadrature amplitude modulation) where M is the modulation order. In DCO-OFDM, a data frame in the form of $X = [0\ s_1\ s_2 ...\ s_{N/2-1}\ 0\ s_{N/2-1}^* ...\ s_2^*\ s_1^*]$ is constructed. The Hermitian symmetry property of frequency-domain vector $\mathbf{X}$ is needed to create a real valued output signal that is used to modulate the LED intensity. The

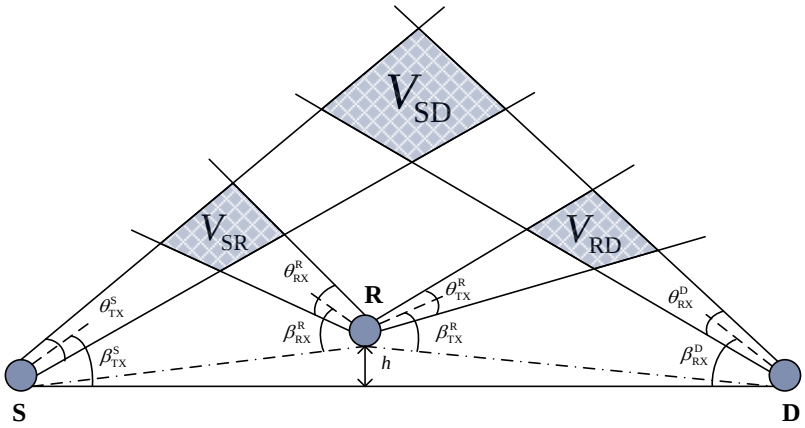

Figure 4: Cooperative UV system.

OFDM modulator applies an N-point Inverse Fast Fourier Transform (IFFT) on $\mathbf{X}$. The output of the IFFT is the time vector to be emitted by LED and is given by $x\left(n\right)=\sum_{i=0}^{N-1}X\left(i\right)e^{j2\pi ni/N}$ where $X\left(i\right)$ denotes the i^{th} element of X . A cyclic prefix (CP) of length $N_g$is appended to eliminate the ISI caused by multipath effect. In the baseband form, the intensity waveform is given by $x(t)=\sum_{n=0}^{L-1}x\left(n\right)\delta(t-nT_s)$, where T_s is the sampling interval and $L=N+N_g$ is the total length of the OFDM symbol. To address the bipolarity, a DC bias is added in order to shift the negative values to positive values before modulating the LED intensity [32]. The resulting optical signal is sent through the UV channel.

We assume that the available OFDM signal energy for cooperative transmission is $2E$,i.e., an average energy of E per transmission phase, to make a fair comparison with point-to-point transmission. Let K_E denote the optimization parameter to control the fraction of information power shared between source and relay. Similarly, let K_L denote the optimization parameter to control fraction of the total DC power shared between these two nodes. In the case of equal power allocation (EPA), we set $K_E=K_L=0.5$. We also define $G_{\text{SR}}=\left|\int_{-\infty}^{+\infty}h_{\text{SR}}\left(t\right)dt\right|^2\Big/\left|\int_{-\infty}^{+\infty}h_{\text{SD}}\left(t\right)dt\right|^2$ and

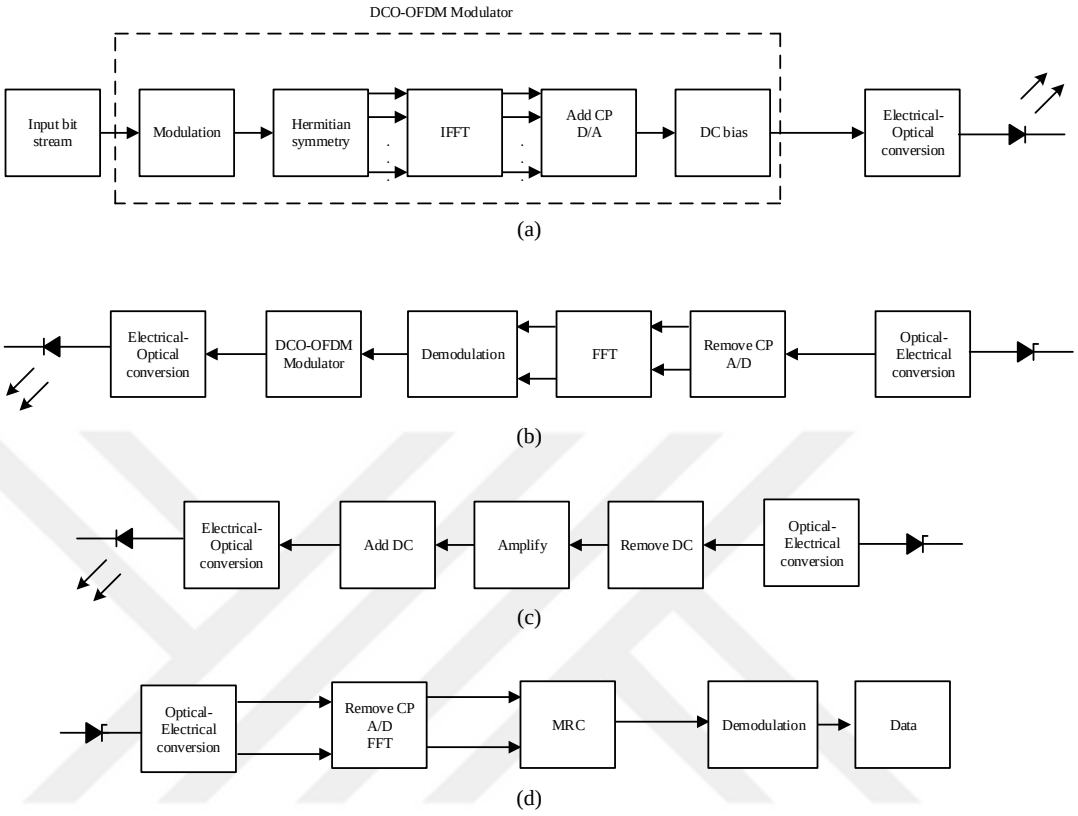

Figure 5: Block diagrams for (a) source; (b) relay in DF mode; (c) relay in AF mode; (d) destination.

$G_{\mathrm{RD}} = \left|\int_{-\infty}^{+\infty} h_{\mathrm{RD}}(t)\,dt\right|^2 \Big/ \left|\int_{-\infty}^{+\infty} h_{\mathrm{SD}}(t)\,dt\right|^2$, respectively, as the geometrical gains for S $\rightarrow$ R link and for R $\rightarrow$ D link where the gain of S $\rightarrow$ D link is normalized as $G_{\mathrm{SD}} = 1$.

The electrical received signal at the destination in the first phase can be written as

$$y_{\mathrm{D}_1}(t) = K_L\sqrt{K_E 2E}\sqrt{G_{\mathrm{SD}}}x(t) \otimes \hat{h}_{\mathrm{SD}}(t) + n_{D_1}(t). \tag{16}$$

In (16), $n_{D_1}(t)$ is the thermal noise modeled as zero mean additive white Gaussian noise (AWGN) with a variance of σ_n^2. Similarly, the electrical received signal at the

relay can be written as

$$y_{\mathrm{R}}(t) = K_L\sqrt{K_E 2E}\sqrt{G_{\mathrm{SR}}}x(t) \otimes \hat{h}_{\mathrm{SR}}(t) + n_{\mathrm{R}}(t), \tag{17}$$

where $n_{\mathrm{R}}(t)$ is the AWGN term with zero mean and variance σ_n^2.

The form of transmitted signal in the second phase depends on the relaying mode. In DF relaying (see Fig. 5.b), the relay node performs the OFDM demodulation and recovers the message signal. Then it performs OFDM modulation, adds DC bias and forwards the resulting toward the destination. Let $\hat{x}_{\mathrm{R}}(t)$ denote the recovered message signal with unit power. The received signal by destination in the second phase can be written as

$$y_{\mathrm{D}_2}(t) = (1 - K_L)\sqrt{G_{\mathrm{RD}}}\sqrt{(1 - K_E)2E}\hat{x}_{\mathrm{R}}(t) \otimes \hat{h}_{\mathrm{RD}}(t) + n_{\mathrm{D}_2}(t), \tag{18}$$

where $n_{\mathrm{D}_2}(t)$ is the AWGN term with zero mean and variance σ_n^2 . Based on (16) and (18), the FFT outputs of the received signals at the i^{th} subcarrier over broadcasting and relaying phases are written as

$$Y_{\mathrm{D}_1}(i) = K_L\sqrt{K_E 2E}\sqrt{G_{\mathrm{SR}}}X(i)\, H_{\mathrm{SD}}(i) + N_{\mathrm{D}_1}(i), \tag{19}$$

$$Y_{\mathrm{D}_2}(i) = (1 - K_L)\sqrt{G_{\mathrm{RD}}}\sqrt{(1 - K_E)2E}\hat{X}_{\mathrm{R}}(i)\, H_{\mathrm{RD}}(i) + N_{\mathrm{D}_2}(i), \tag{20}$$

where $y_{\mathrm{D}_1}(n) \overset{\mathrm{FFT}}{\leftrightarrow} Y_{\mathrm{D}_1}(i)$, $x(n) \overset{\mathrm{FFT}}{\leftrightarrow} X(i)$, $\hat{h}_{\mathrm{SD}}(n) \overset{\mathrm{FFT}}{\leftrightarrow} H_{\mathrm{SD}}(i)$, $n_{\mathrm{D}_1}(n) \overset{\mathrm{FFT}}{\leftrightarrow} N_{\mathrm{D}_1}(i)$, $y_{\mathrm{D}_2}(n) \overset{\mathrm{FFT}}{\leftrightarrow} Y_{\mathrm{D}_2}(i)$, $\hat{x}_{\mathrm{R}}(n) \overset{\mathrm{FFT}}{\leftrightarrow} \hat{X}_{\mathrm{R}}(i)$, $\hat{h}_{\mathrm{RD}}(n) \overset{\mathrm{FFT}}{\leftrightarrow} H_{\mathrm{RD}}(i)$ and $n_{\mathrm{D}_2}(n) \overset{\mathrm{FFT}}{\leftrightarrow} N_{\mathrm{D}_2}(i)$. These signals are fed to the MRC to yield $\hat{X}(i)$.

In AF relaying (see Fig. 5.c), first the DC component in the electrical signal is removed. Then the relay node scales the energy of the intensity waveform to $(1 - K_E)\,2E$. The amplification gain in electrical domain is $A = \sqrt{(1 - K_E)\,2E / (2EK_E K_L^2 G_{\mathrm{SR}} + \sigma_n^2}$ Finally, the relay adds a DC term and performs electrical-to-optical conversion via LED. The received electrical signal at the destination during the relaying phase is

given by

$$y_{\mathrm{D}_2}(t) = (1 - K_L)\, A\sqrt{G_{\mathrm{RD}}} y_{\mathrm{R}}(t) \otimes \hat{h}_{\mathrm{RD}}(t) + n_{\mathrm{D}_2}(t). \tag{21}$$

The corresponding frequency domain signal is given by

$$Y_{\mathrm{D}_2}(i) = (1 - K_L)\, A\sqrt{G_{\mathrm{RD}}} Y_{\mathrm{R}}(i)\, H_{\mathrm{RD}}(i) + N_{\mathrm{D}_2}(i), \tag{22}$$

where $y_{\mathrm{R}}(n) \overset{\mathrm{FFT}}{\leftrightarrow} Y_{\mathrm{R}}(i)$and $\hat{h}_{\mathrm{RD}}(n) \overset{\mathrm{FFT}}{\leftrightarrow} H_{\mathrm{RD}}(i)$. The received signals in (19) and (22) are fed to the MRC to yield the decision.

3.3 BER Performance Analysis and Optimization

In this section, we first study the BER performance of relay-assisted OFDM UV systems for both DF and AF relaying modes. Then, we minimize the BER through optimal power allocation (OPA), i.e., determining optimal values of K_E and K_L.

End-to-end SNR at the output of MRC for the i^{th} subcarrier can be written as

$$SNR_i = SNR_{\mathrm{SD},i} + SNR_{\mathrm{SRD},i}, \tag{23}$$

where $SNR_{\mathrm{SD},i} = 2\gamma K_{E,i} K_{L,i}^2 |H_{\mathrm{SD}}(i)|^2$ with $\gamma = E/\sigma_n^2$. $SNR_{\mathrm{SRD},i}$ is the overall SNR of the relaying path, i.e., the SNR for an equivalent single-hop OFDM link that produces the same performance as two-hop link, and its form depends on the relaying technique. The approximate BER for an OFDM system employing linear modulation schemes such as QAM is given by [33]

$$BER \approx \frac{1}{N/2-1} \sum_{i=1}^{N/2-1} BER_i, \tag{24}$$

where BER_i is the BER of the i^{th} subcarrier, $i = 1, ..., N/2-1$. BER_i is given by [33]

$$BER_i \approx \frac{4}{\log_2 M} \left(1 - \frac{1}{\sqrt{M}}\right) Q\left(\sqrt{\frac{3SNR_i}{M-1}}\right). \tag{25}$$

SNR_i can be written as a function of BER_i as

$$SNR_i = f(BER_i) = \left(\frac{M-1}{3}\right) \left(Q^{-1}\left(\frac{BER_i \log_2 M}{4}\left(1 - \frac{1}{\sqrt{M}}\right)^{-1}\right)\right)^2. \tag{26}$$

Since $Q(\cdot)$ is a decreasing function, minimization of (25) is equivalent to maximization of (26). This would yield different optimal K_L and K_E values for each subcarrier. The UV channel is of deterministic nature and variations in frequency domain are relatively small, see for example Fig.6 of Section 3.3.1. Therefore, we first obtain optimal values for each subcarrier, i.e., $K_{L,i}^{\text{opt}}$ and $K_{E,i}^{\text{opt}}$ for $i = 1, ..., N/\ .2 - 1$, then take the average over all subcarriers through

$$K_{L,\text{avg}} = \frac{1}{N/2-1} \sum_{i=1}^{N/2-1} K_{L,i}^{\text{opt}}, \tag{27.a}$$

$$K_{E,\text{avg}} = \frac{1}{N/2-1} \sum_{i=1}^{N/2-1} K_{E,i}^{\text{opt}}, \tag{27.b}$$

and finally use the resulting average values in our system.

The form of SNR_i in (23) depends on the relaying mode due to the second term. Details of the derivations for both DF and AF relaying are found in the following.

3.3.1 DF Relaying

In DF relaying, the BER for the relaying path is given by [34]

$$BER_{\text{SRD},i} = BER_{\text{SR},i}\left(1 - BER_{\text{RD},i}\right) + BER_{\text{RD},i}\left(1 - BER_{\text{SR},i}\right), \tag{28}$$

where $BER_{\text{SR},i}$ and $BER_{\text{RD},i}$ are the BERs associated with S $\rightarrow$ R and R $\rightarrow$ D links for the i^{th} subcarrier. Based on (25) and (26), we can write

$$SNR_{\text{SRD},i} = f\left(f^{-1}\left(SNR_{\text{SR},i}\right)\right)\left(1 - f^{-1}\left(SNR_{\text{RD},i}\right)\right) + f^{-1}\left(SNR_{\text{RD},i}\right)\left(1 - f^{-1}\left(SNR_{\text{SR},i}\right)\right), \tag{29}$$

where $SNR_{\text{SR},i} = 2\gamma G_{\text{SR}} K_{E,i} K_{L,i}^2 \left|H_{\text{SR}}(i)\right|^2$ and $SNR_{\text{RD},i} = 2\gamma G_{\text{RD}}\left(1 - K_{E,i}\right)\left(1 - K_{L,i}\right)^2 \left|H_{\text{RD}}(i)\right|^2$.

Replacing (29) in (23) yields the end-to-end SNR for DF relaying. The optimization of the resulting expression is mathematically intractable. In an effort to find a

closed-form solution, we approximate the end-to-end SNR as [34]

$$SNR_i \approx SNR_{\mathrm{SD},i} + \min\left\{SNR_{\mathrm{SR},i}, SNR_{\mathrm{RD},i}\right\}. \tag{30}$$

For the optimization of (30), we investigate two separate cases, namely $SNR_{\mathrm{SR},i} < SNR_{\mathrm{RD},i}$ and $SNR_{\mathrm{SR},i} > SNR_{\mathrm{RD},i}$. Our optimization problem for the first case, i.e., $SNR_{\mathrm{SR},i} < SNR_{\mathrm{RD},i}$, can be written as

$$\max_{s.t.\ \Delta_1\left(K_{L,i},K_{E,i}\right)\leq\frac{G_{\mathrm{RD}}|H_{\mathrm{RD}}(i)|^2}{G_{\mathrm{SR}}|H_{\mathrm{SR}}(i)|^2}} f_1\left(K_{L,i},K_{E,i}\right) = \left(G_{\mathrm{SR}}|H_{\mathrm{SR}}\left(i\right)|^2 \,/\, |H_{\mathrm{SD}}\left(i\right)|^2 + 1\right) K_{E,i}K_{L,i}^2, \tag{31}$$

where $\Delta_1\left(K_{L,i},K_{E,i}\right) = K_{E,i}K_{L,i}^2 \big/ [(1-K_{E,i})\left(1-K_{L,i}\right)^2]$. For the second case, i.e., $SNR_{\mathrm{SR},i} > SNR_{\mathrm{RD},i}$, our optimization problem is stated as

$$\begin{aligned}\max_{s.t.\ \Delta_2\left(K_{L,i},K_{E,i}\right)\leq\frac{G_{\mathrm{SR}}|H_{\mathrm{SR}}(i)|^2}{G_{\mathrm{RD}}|H_{\mathrm{RD}}(i)|^2}} f_2\left(K_{L,i},K_{E,i}\right) &= K_{E,i}K_{L,i}^2 + \left(G_{\mathrm{RD}}|H_{\mathrm{SR}}\left(i\right)|^2 \,/\, |H_{\mathrm{SD}}\left(i\right)|^2\right) \\ &\times \left(1-K_{E,i}\right)\left(1-K_{L,i}\right)^2, \end{aligned} \tag{32}$$

where $\Delta_2\left(K_{L,i},K_{E,i}\right) = \left(1-K_{E,i}\right)\left(1-K_{L,i}\right)^2 \big/ K_{E,i}K_{L,i}^2$. Using Lagrangian method (see Appendix for the details), in both cases optimized values of $K_{L,i}$ and $K_{E,i}$ are obtained as

$$K_{L,i}^{\mathrm{opt}} = K_{E,i}^{\mathrm{opt}} = \frac{\sqrt[3]{G_{\mathrm{RD}}\left|H_{\mathrm{RD}}\left(i\right)\right|^2 \,/\, .\left(G_{\mathrm{SR}}\left|H_{\mathrm{SR}}\left(i\right)\right|^2\right)}}{1+\sqrt[3]{G_{\mathrm{RD}}\left|H_{\mathrm{RD}}\left(i\right)\right|^2 \,/\, .\left(G_{\mathrm{SR}}\left|H_{\mathrm{SR}}\left(i\right)\right|^2\right)}}. \tag{33}$$

As it can be seen, (33) is independent of γ. This is due to the approximation in (30).

As an example, we consider a UV link with a distance of $d = 100$ m. The relay is deployed 40 m apart from the source on the direct line connecting the source and destination. We assume $N = 512$, $N_g = 5$, and 16-QAM. The transmitter and receiver parameters are given by $\left(\beta_{\mathrm{TX}}^{\mathrm{S}}, \beta_{\mathrm{RX}}^{\mathrm{D}}, \theta_{\mathrm{TX}}^{\mathrm{S}}, \theta_{\mathrm{RX}}^{\mathrm{D}}\right) = (90^\circ, 90^\circ, 20^\circ, 30^\circ)$ and $\left(\beta_{\mathrm{TX}}^{\mathrm{R}}, \beta_{\mathrm{RX}}^{\mathrm{R}}, \theta_{\mathrm{TX}}^{\mathrm{R}}, \theta_{\mathrm{RX}}^{\mathrm{R}}\right) = (80^\circ, 80^\circ, 20^\circ, 30^\circ)$. We set $A_{\mathrm{R}} = 1.77$ cm^2, $k_e = 1.39$ km^{-1} and $k_s = 0.49$ km^{-1} so the single scatter assumption holds i.e. $\tau_s = k_s d = 0.049 \leq 0.1$. We

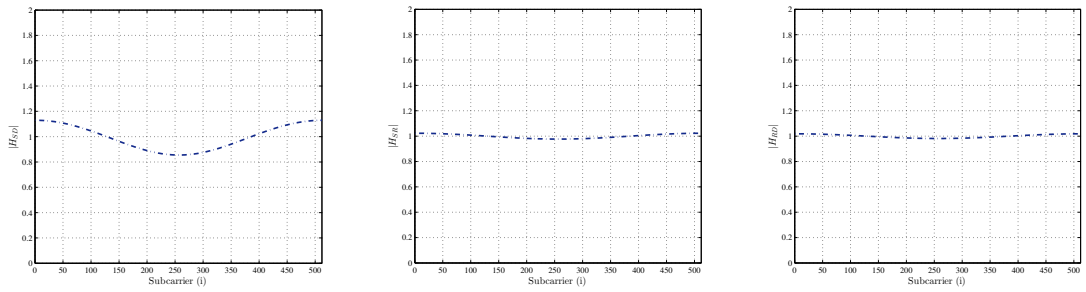

(a) (b) (c)

Figure 6: Channel transfer function for (a) S $\rightarrow$ D , (b) S $\rightarrow$ R and (c) R $\rightarrow$ D links.

Table 2: Values of optimal K_L and K_E for DF relaying.

	$\gamma = 0$ dB	$\gamma =$ 4 dB	$\gamma =$ 8 dB	$\gamma =$ 12 dB	$\gamma =$ 16 dB	$\gamma =$ 20 dB	$\gamma =$ 24 dB	Eq. (33)
K_L	0.4086	0.4004	0.3973	0.3963	0.3959	0.3958	0.3957	0.3949
K_E	0.4086	0.4004	0.3973	0.3962	0.3959	0.3957	0.3957	0.3949

use truncated sinc pulse as pulse shaping filter. Sampling interval is $T_s = 0.5$ μsec. For these parameters, we calculate $G_{\text{SR}} = 23.3192$ dB and $G_{\text{RD}} = 17.7604$ dB. The channel transfer function is illustrated in Fig.6 . As earlier mentioned, it is observed that variations of the UV channel in frequency domain are relatively small. This justifies the use of average values in practice.

From (33), we first calculate $K_{L,i}^{\text{opt}}$ and $K_{E,i}^{\text{opt}}$ for $i = 1, ..., N/2 - 1$ and then the averaging calculated through (27) yields $K_{L,\text{avg}} = K_{E,\text{avg}} = 0.3949$. To check the accuracy of our approach, we also determine optimal values for K_L and K_E through direct numerical optimization of (24) in conjunction with (23) and (29). These results are provided in Table 2[1]. It is observed that our closed form solution in (33) provides a good match to the numerically optimized values.

[1]The accuracy of (33) has been investigated for a variety of system configurations. Table 2 is provided only as an example.

3.3.2 AF Relaying

In AF relaying, the overall SNR of the relaying path can be written as

$$SNR_{\mathrm{SRD},i} = \frac{SNR_{\mathrm{SR},i} SNR_{\mathrm{RD},i}}{SNR_{\mathrm{SR},i} + SNR_{\mathrm{RD},i} + 1}. \tag{34}$$

Replacing (34) in (23) and after some manipulations, end-to-end SNR at the output of MRC is obtained as

$$SNR_i = 2\gamma K_{E,i} K_{L,i}^2 \left|H_{\mathrm{SD}}(i)\right|^2 + \frac{2\gamma K_{E,i} K_{L,i}^2 G_{\mathrm{SR}} \left|H_{\mathrm{SR}}(i)\right|^2}{\frac{2\gamma K_{E,i} K_{L,i}^2 G_{\mathrm{SR}} |H_{\mathrm{SR}}(i)|^2 + 1}{2\gamma \left(1-K_{E,i}\right)\left(1-K_{L,i}\right)^2 G_{\mathrm{RD}} |H_{\mathrm{RD}}(i)|^2} + 1}. \tag{35}$$

The maximization of (35) with respect to optimization parameters $K_{L,i}$ and $K_{E,i}$ is mathematically intractable. In the following, we pursue a sub-optimal solution in an effort to find a closed form expression.

First, we focus on the second term in (35). It can be approximated as

$$SNR_{\mathrm{SRD},i} \approx \frac{2\gamma K_{E,i} \left(1-K_{E,i}\right) K_{L,i}^2 \left(1-K_{L,i}\right)^2 G_{\mathrm{SR}} \left|H_{\mathrm{SR}}(i)\right|^2 G_{\mathrm{RD}} \left|H_{\mathrm{RD}}(i)\right|^2}{K_{E,i} K_{L,i}^2 G_{\mathrm{SR}} \left|H_{\mathrm{SR}}(i)\right|^2 + \left(1-K_{E,i}\right)\left(1-K_{L,i}\right)^2 G_{\mathrm{RD}} \left|H_{\mathrm{RD}}(i)\right|^2}. \tag{36}$$

Note that the optimization of (36) is independent of γ.Taking the derivative of (36) with respect to $K_{E,i}$ and equating it to zero, we have

$$\bar{K}_{E,i}^{\mathrm{opt}} = \frac{G_{\mathrm{RD}} \left|H_{\mathrm{SR}}(i)\right|^2 \left(1-K_{L,i}\right)^2 - K_{L,i}\left(1-K_{L,i}\right)\sqrt{G_{\mathrm{SR}} \left|H_{\mathrm{SR}}(i)\right|^2 G_{\mathrm{RD}} \left|H_{\mathrm{RD}}(i)\right|^2}}{G_{\mathrm{RD}} \left|H_{\mathrm{RD}}(i)\right|^2 \left(1-K_{L,i}\right)^2 - G_{\mathrm{SR}} \left|H_{\mathrm{SR}}(i)\right|^2 K_{L,i}^2}. \tag{37}$$

Then we take derivative with respect to $K_{L,i}$ and equate it to zero i.e., $\partial SNR_{\mathrm{SRD},i}/\partial K_{L,i}{}_{K_{E,i}=\bar{K}_{E,i}^{\mathrm{opt}}} = 0$. The optimum value for $K_{L,i}$ can be found as

$$K_{L,i}^{\mathrm{opt}} = \frac{-W}{3\left(G_{\mathrm{SR}} \left|H_{\mathrm{SR}}(i)\right|^2 - G_{\mathrm{RD}} \left|H_{\mathrm{RD}}(i)\right|^2\right)} \left[1 - \frac{1}{2}\left(C + \bar{C}\right) + \frac{\sqrt{3}i}{2}\left(C - \bar{C}\right)\right] \text{ for } G_{\mathrm{SR}} \neq G_{\mathrm{RD}}, \tag{38}$$

where W, C,$\bar{C}$,Δ_0 and Δ_1 are respectively defined as

$$W = 3G_{\mathrm{RD}} \left|H_{\mathrm{RD}}(i)\right|^2 - \sqrt{G_{\mathrm{RD}} \left|H_{\mathrm{RD}}(i)\right|^2 G_{\mathrm{SR}} \left|H_{\mathrm{SR}}(i)\right|^2},$$

Table 3: Values of optimal K_L and K_E for AF relaying.

	$\gamma = 0$ dB	$\gamma =$ 4 dB	$\gamma =$ 8 dB	$\gamma =$ 12 dB	$\gamma =$ 16 dB	$\gamma =$ 20 dB	$\gamma =$ 24 dB	Eq. (38)& (39)
K_L	0.4231	0.4226	0.4224	0.4224	0.4225	0.4225	0.4225	0.4207
K_E	0.4231	0.4226	0.4225	0.4224	0.4224	0.4225	0.4225	0.4207

$$C = \sqrt[3]{0.5\left(\Delta_1 + \sqrt{\Delta_1^2 - 4\Delta_0^3}\right)},$$

$$\bar{C} = \sqrt[3]{0.5\left(\Delta_1 - \sqrt{\Delta_1^2 - 4\Delta_0^3}\right)},$$

$$\Delta_0 = 1 + \frac{3\left(G_{\mathrm{SR}}\left|H_{\mathrm{SR}}\left(i\right)\right|^2 - G_{\mathrm{RD}}\left|H_{\mathrm{RD}}\left(i\right)\right|^2\right)}{W},$$

$$\Delta_1 = 2 + \frac{9\left(G_{\mathrm{SR}}\left|H_{\mathrm{SR}}\left(i\right)\right|^2 - G_{\mathrm{RD}}\left|H_{\mathrm{RD}}\left(i\right)\right|^2\right)}{W}\left[1 + \frac{3G_{\mathrm{RD}}\left|H_{\mathrm{RD}}\left(i\right)\right|^2}{W^2}\right].$$

Now if we substitute $K_{L,i}^{\mathrm{opt}}$ in (37) , we obtain

$$K_{E,i}^{\mathrm{opt}} = \frac{G_{\mathrm{RD}}\left|H_{\mathrm{RD}}\left(i\right)\right|^2\left(1 - K_{L,i}^{\mathrm{opt}}\right)^2 - K_{L,i}^{\mathrm{opt}}\left(1 - K_{L,i}^{\mathrm{opt}}\right)\sqrt{G_{\mathrm{RD}}\left|H_{\mathrm{RD}}\left(i\right)\right|^2 G_{\mathrm{SR}}\left|H_{\mathrm{SR}}\left(i\right)\right|^2}}{G_{\mathrm{RD}}\left|H_{\mathrm{RD}}\left(i\right)\right|^2\left(1 - K_{L,i}^{\mathrm{opt}}\right)^2 - G_{\mathrm{SR}}\left|H_{\mathrm{SR}}\left(i\right)\right|^2\left(K_{L,i}^{\mathrm{opt}}\right)^2}. \tag{39}$$

The first term in SNR_i in (35) is optimized when the values of K_L and K_E are set to one. In this case, average SNR per transmission phase is γ. Our aim is to achieve a larger end-to-end SNR through relay-assisted transmission. To make sure that cooperative transmission outperforms direct transmission, values of $K_{L,i}^{\mathrm{opt}}$ and $K_{E,i}^{\mathrm{opt}}$ obtained through (38) and (39) must satisfy the condition $1\,/\,.(2\,(N\,/\,.2-1))\sum_{i=1}^{N\,/\,.2-1} SNR_i > \gamma$ where the factor of 2 is introduced to take into account two-phase transmission. Otherwise, the optimum values for K_L and K_E are set to one.

In Table 3[2], we present the optimal values of K_L and K_E through numerical optimization of (24) in conjunction with (35). We consider the same system parameters as in Section 3.3.1. We further include the values obtained from the derived closed form expressions in (38) and (39) after calculating their average through (27). It is observed that our closed form solutions provide a good match with numerically optimized values.

3.4 Bit Loading for Throughput Maximization

In the previous section, we have discussed optimal power allocation between source and relay node. At each node, we have assumed that the same power level is allocated to each subcarrier and the same modulation order (size) is used. In this section, we consider a variable-rate system and consider the use of different modulation orders which is also known as bit loading in the literature [33].

Let BER_t denote a targeted value of BER. The specific value can be chosen based on the quality of service (QoS) requirements. Furthermore, define $SNR_{i,k}^{th}$ as the threshold SNR which is required to reach BER_t for the i^{th} subcarrier. Based on (26), we can define $SNR_{i,k}^{th}$ as

$$SNR_{i,k}^{th} = \left(\frac{2^k - 1}{3\left|H_{\text{SD}}\left(i\right)\right|^2}\right)\left(Q^{-1}\left(\frac{BER_t k}{4}\left(1 - \frac{1}{\sqrt{2^k}}\right)^{-1}\right)\right)^2,$$
$$k = 1, 2, ..., K;\ i = 1, ..., N/2 - 1 \tag{40}$$

where $k = \log_2 M$.

Let b_i denote the number of bits loaded on the i^{th} subcarrier and Γ_i denote the SNR of the i^{th} subcarrier. b_i can take a maximum value of $k \in \{1, 2, ..., K\}$ bits that satisfies the condition $\Gamma_i - SNR_{k,i}^{th} \geq 0$. Minimum power is consumed for the limiting

[2]The accuracy of (38) and (39) have been investigated for a variety of system configurations. Table 3 is provided only as an example.

case i.e., $\Gamma_i \in \left\{SNR_{k,i}^{th},\ k = 1, 2, ..., \mathrm{K}\right\}$. In this case, the throughput is given by

$$R = \frac{1}{2(N/2-1)} \sum_{i=1}^{N/2-1} b_i, \tag{41}$$

where the factor of 2 is introduced to take into account two-phase transmission. Optimization problem can be therefore expressed as

$$\max_{b_i} \quad \left\{ R_{\text{total}} = \sum_{i=1}^{N/2-1} b_i \right\}, \tag{42}$$
$$\sum_{\mathrm{i=1}}^{\mathrm{N/2-1}} \Gamma_{\mathrm{i}} \leq \sum_{\mathrm{i=1}}^{\mathrm{N/2-1}} \mathrm{SNR_i}$$

where SNR_i is defined in (30) and (35) respectively for DF and AF relaying. Define $\Delta SNR_{i,k}$ as [35]

$$\Delta SNR_{i,k} = \begin{cases} SNR_{i,1}^{th} & k = 1 \\ SNR_{i,k}^{th} - SNR_{i,k-1}^{th} & k = 2, ..., \mathrm{K} \end{cases}, \tag{43}$$

where $\Delta SNR_{i,k} \leq \Delta SNR_{i,k+1}$. If the modulation order of the i^{th} subcarrier is $M-\text{QAM}$ with $M = 2^{b_i}$, the SNR of the i^{th} subcarrier is then given by $\Gamma_i = \sum_{k=1}^{b_i} \Delta SNR_{i,k}$. In this case, the constraint (42) can be written as

$$\sum_{i=1}^{N/2-1} \sum_{k=1}^{b_i} \Delta SNR_{i,k} \leq \sum_{i=1}^{N/2-1} SNR_i. \tag{44}$$

The optimization problem in (42) can be solved as follows: First, we sort the $(N/2-1)K$ values of $\Delta SNR_{i,k}$ in ascending order. Denote the ordered sequence as $\Upsilon_1 \leq \Upsilon_2 \leq ... \leq \Upsilon_{(N/2-1)\mathrm{K}}$. We can then find the maximum value of R_{total} subject to $\sum_{i=1}^{R_{\text{total}}} \Upsilon_i \leq \sum_{i=1}^{N/2-1} SNR_i$.

3.5 Numerical Results and Discussions

In this section, we present simulation results to evaluate the performance of co-operative OFDM UV system under consideration. The performance of point-to-point (direct) OFDM transmission is also included as a benchmark.

In the first part, to make a fair comparison between BER performance of direct and cooperative transmission, we keep the throughput fixed hence the direct transmission is simulated with 4-QAM while cooperative transmission is simulated with 16-QAM. In the simulation study, we assume $N = 512$ subcarriers with a CP length of $N_g = 5$. Unless otherwise stated, similar to Section 3.3, we assume $\beta_{\mathrm{TX}}^{\mathrm{S}} = \beta_{\mathrm{RX}}^{\mathrm{D}} = 90°$, $\beta_{\mathrm{RX}}^{\mathrm{R}} = \beta_{\mathrm{TX}}^{\mathrm{R}} = 80°$, $\theta_{\mathrm{TX}}^{\mathrm{S}} = \theta_{\mathrm{TX}}^{\mathrm{R}} = 20°$ and $\theta_{\mathrm{RX}}^{\mathrm{R}} = \theta_{\mathrm{RX}}^{\mathrm{D}} = 30°$. The link distance is 100 m and a fixed SNR of $\gamma = E/\ \sigma_n^2 = 6$ dB is considered.

In Fig. 7, we demonstrate the performance improvements through OPA and also discuss the effect of relay location. We assume that the relay node is located on the line connecting the source and the destination, i.e., h=0, and illustrate the BER performance of cooperative system with respect to the distance between the source and the relay. We consider three cases with various values of relay/destination receiver FOVs: (a) $\theta_{\mathrm{RX}}^{\mathrm{R}} = \theta_{\mathrm{RX}}^{\mathrm{D}} = 30°$, (b) $\theta_{\mathrm{RX}}^{\mathrm{R}} = 30°$, $\theta_{\mathrm{RX}}^{\mathrm{D}} = 40°$, (c) $\theta_{\mathrm{RX}}^{\mathrm{R}} = 40°$, $\theta_{\mathrm{RX}}^{\mathrm{D}} = 30°$. EPA with $K_L = K_E = 0.5$ is also considered as a benchmark. For case (a), the best performance is achieved when the relay is located at the midpoint, i.e., 50 m from the source. In this position, EPA and OPA performances converge. However, in other relay locations, OPA provides significant improvements over EPA. In case (b), we consider a larger FOV for the destination node, therefore the performance of point-to-point transmission is improved with respect to case (a). In this case, we have higher geometrical gain in R $\rightarrow$ D link and expect to see the best performance when relay is close to the source. In fact, the best performance is achieved when relay is located around 30 m away from the source. It can be also observed from Fig.10.b that while AF relaying provides no or small improvement in comparison with point-to-point transmission, DF significantly improves the performance. However, in most cases, OPA is required to realize the advantages of cooperative transmission. In case (c), we consider a larger FOV for the relay node which yields a higher geometrical gain in S $\rightarrow$ R link. As a result, the best performance is achieved when the relay is around

70 m far from the source. It is observed from Fig.7.c that OPA schemes (for both AF and DF relaying) always outperform point-to-point transmission and EPA scheme is better than point-to-point transmission for most relay locations. Our observations from Fig.7 indicate that the performance of cooperative system is highly dependent on system geometry and relay location. In most cases, DF relaying outperforms AF counterpart. Also, for some configurations, it is observed that cooperative system with EPA is not able to outperform the point-to-point transmission and OPA is required to realize the advantages of cooperative transmission.

In Fig. 8, we further investigate the impact of relay location considering different values of h. The projection of the relay location on direct line connecting source and destination is fixed and 40 m away from the source. We consider two different values for $\theta_{\mathrm{RX}}^{\mathrm{R}}$ $(30^{\circ},\ 40^{\circ})$ and assume DF and AF relaying with OPA. Relatively large performance gains over point-to-point transmission are observed for small h values, i.e., when the relay is close to the direct line. The gains diminish as h increases. It is also observed that, for a given value of h, increasing the relay FOV ($\theta_{\mathrm{RX}}^{\mathrm{R}}$) yields some additional performance improvements.

In Fig. 9, we investigate the effect of relay receiver FOV ($\theta_{\mathrm{RX}}^{\mathrm{R}}$) and transmitter elevation angle ($\beta_{\mathrm{TX}}^{\mathrm{R}}$) on the BER. The relay is located at 40 m from the source on the direct line connecting source and destination. In Fig.9.a we assume $\left(\beta_{\mathrm{TX}}^{\mathrm{R}}, \beta_{\mathrm{RX}}^{\mathrm{R}}\right) = (80^{\circ}, 80^{\circ})$ and vary $\theta_{\mathrm{RX}}^{\mathrm{R}}$. It is observed from Fig.9.a that while EPA provides limited improvement with wider FOV, OPA brings significant performance improvements. For example, in AF relaying with OPA, the BER decreases from 3.8×10^{-3} to 1.4×10^{-4} when $\theta_{\mathrm{RX}}^{\mathrm{R}}$ changes from 20° to 40° . This indicates improvement by approximately a factor of 27. In DF OPA, an improvement by a factor of 245 is obtained for the same $\theta_{\mathrm{RX}}^{\mathrm{R}}$ values. In Fig.9.b, we assume $\left(\theta_{\mathrm{RX}}^{\mathrm{R}}, \beta_{\mathrm{RX}}^{\mathrm{R}}\right) = (30^{\circ}, 90^{\circ})$ and vary the value of $\beta_{\mathrm{TX}}^{\mathrm{R}}$. It is observed that while EPA does not bring much improvement after a certain degree, cooperative transmission with OPA outperforms point-to-point transmission.

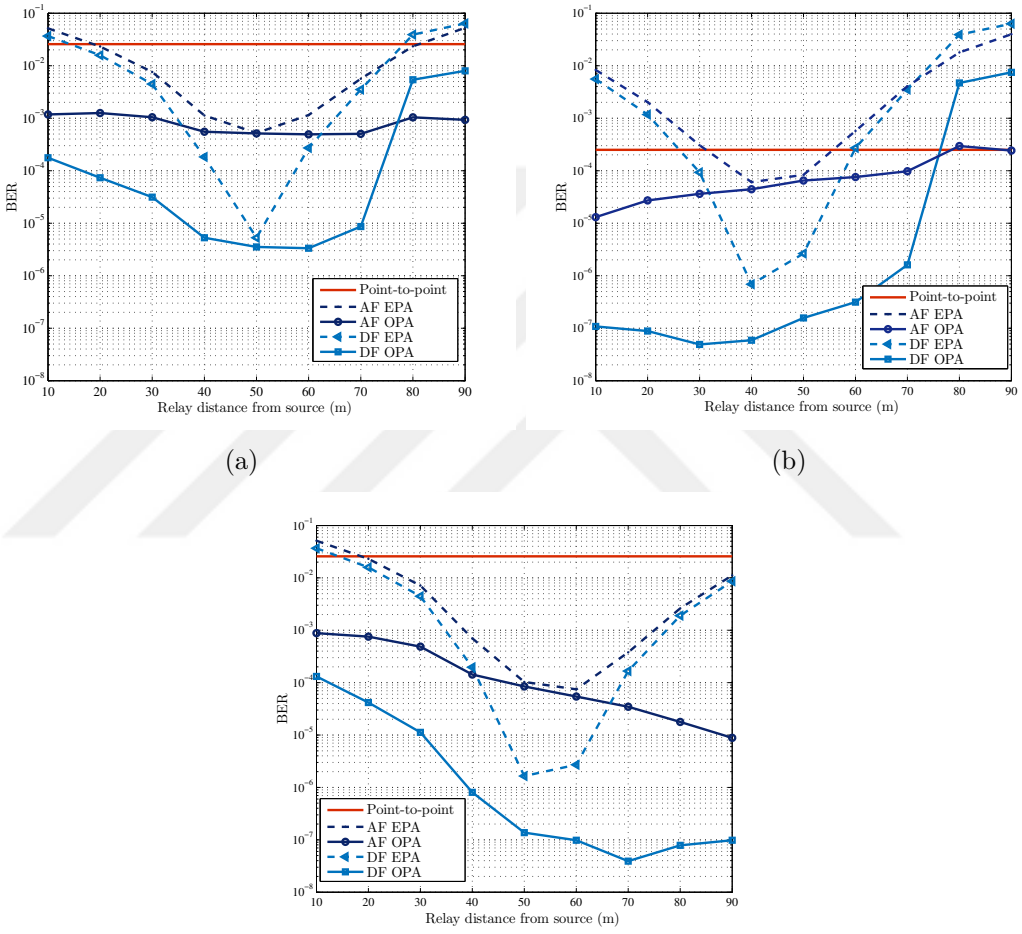

Figure 7: BER versus relay location for (a)$\theta^{\mathrm{R}}_{\mathrm{RX}} = \theta^{\mathrm{D}}_{\mathrm{RX}} = 30°$, (b)$\theta^{\mathrm{R}}_{\mathrm{RX}} = 30°$, $\theta^{\mathrm{D}}_{\mathrm{RX}} = 40°$ (c) $\theta^{\mathrm{R}}_{\mathrm{RX}} = 40°$, $\theta^{\mathrm{D}}_{\mathrm{RX}} = 30°$.

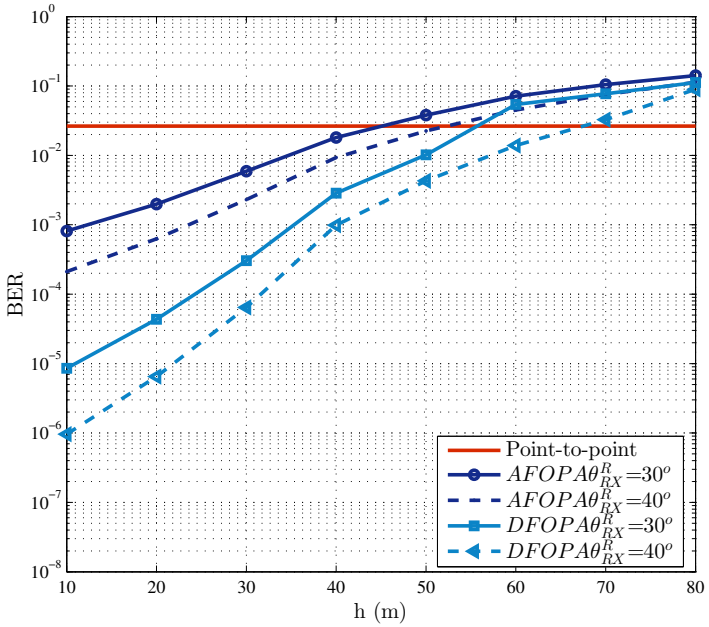

Figure 8: BER versus different h values.

For AF relaying with OPA assumption, an improvement by a factor of 13 is obtained when $\beta_{\mathrm{TX}}^{\mathrm{R}}$ decreases from 80° to 60°. More improvement is obtained by DF relaying with OPA.

In Fig. 10, we illustrate BER performance with respect to SNR for different values of destination FOV ($\theta_{\mathrm{RX}}^{\mathrm{D}}$). We assume that the relay is located 40 m away from source on the direct line connecting source and destination. As the destination FOV increases, a better performance is achieved. Specifically, to achieve BER=10^{-5}, an SNR of 13 dB is required for point-to-point transmission with $\theta_{\mathrm{RX}}^{\mathrm{D}} = 30°$. This reduces to 8 dB for $\theta_{\mathrm{RX}}^{\mathrm{D}} = 40°$. With AF relaying, OPA requires 8.2 dB and 6.8 dB respectively for $\theta_{\mathrm{RX}}^{\mathrm{D}} = 30°$ and $\theta_{\mathrm{RX}}^{\mathrm{D}} = 40°$ indicating performance improvements of 4.8 dB and 1.2 dB over point-to-point transmission. This improvement further climbs to 6.5 dB and 3.8 dB for DF relaying.

In Fig. 11, we present the throughput for cooperative OFDM UV system with bit loading for a targeted BER value of 10^{-3}. We consider QAM with modulation sizes

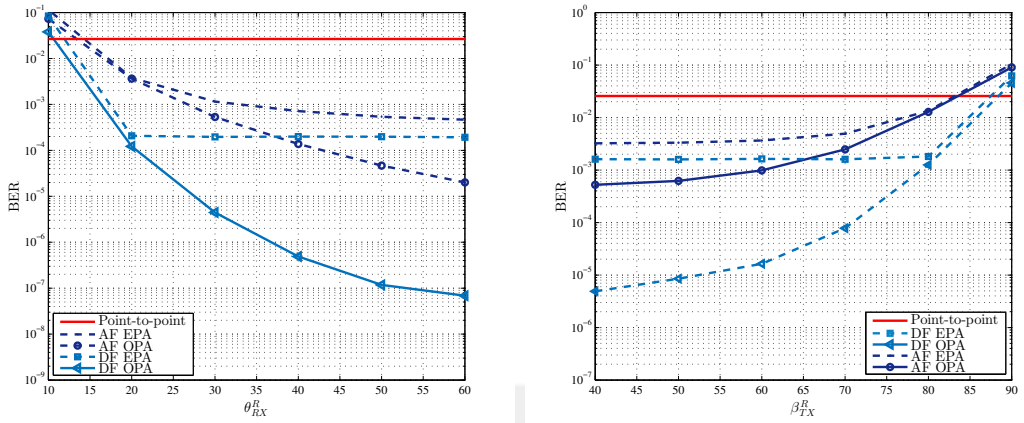

(a) (b)

Figure 9: BER versus (a) relay receiver FOV ($\theta^{\mathrm{R}}_{\mathrm{RX}}$) (b) relay transmitter elevation angle ($\beta^{\mathrm{R}}_{\mathrm{TX}}$).

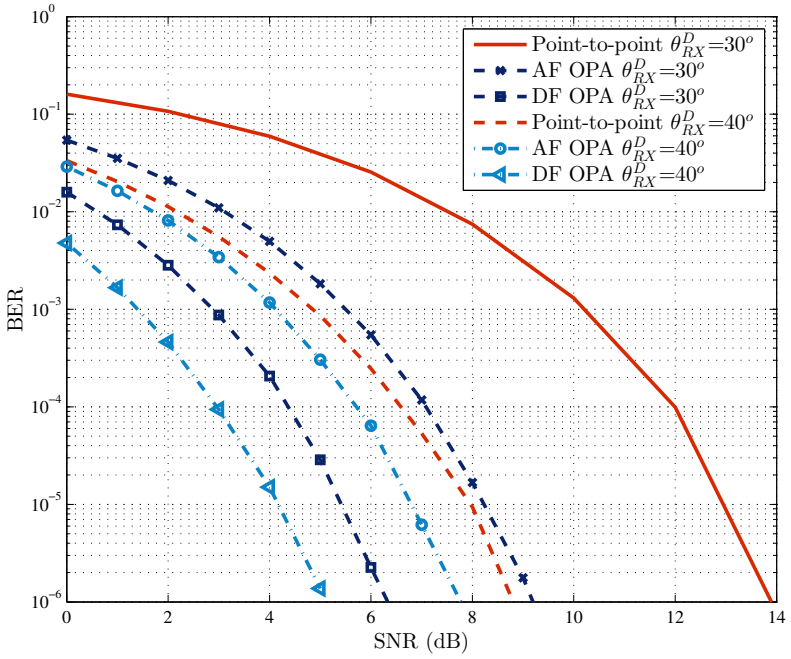

Figure 10: BER versus SNR for different values of destination receiver FOV ($\theta^{\mathrm{D}}_{\mathrm{RX}}$).

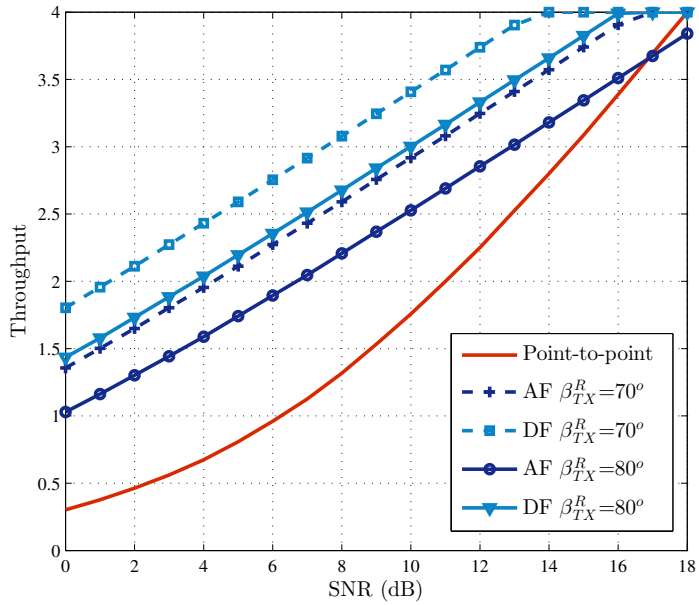

Figure 11: Throughput for cooperative transmission with bit loading.

$M = 2, 4, ..., 256$. It is observed that cooperative transmission in general provides more throughput in comparison with point-to-point transmission. For example, at SNR=5 dB, point-to-point transmission achieves a throughput of 0.8 bits which increases to 1.7 and 2.2 bits for AF and DF relaying indicating more than 2 times improvement over point-to-point counterpart. In general, DF relaying outperforms AF counterpart for all SNR regime. It is also observed that employment of a relay with smaller elevation angle ($\beta_{\mathrm{TX}}^{\mathrm{R}}$) yields better performance.

CHAPTER IV

RELAY-ASSISTED NLOS ULTRAVIOLET COMMUNICATIONS OVER TURBULENCE CHANNELS

4.1 Introduction

In the previous chapter, the effects of turbulence are ignored. In this chapter, we investigate the performance of relay-assisted UV systems over turbulence induced frequency-flat fading channels. Specifically, we consider a multi-hop UV system with DF relaying. Based on the asymptotic outage expressions, we present a diversity gain analysis and obtain the diversity order as a function of link distance and system parameters. Our results show that, with proper choice of these parameters, the turbulence variance for NLOS link can be lower than that of LOS link. This in return yields higher diversity gains. We present numerical results to confirm the accuracy of our derivations and discuss the effect of several system parameters on the outage probability and diversity gain.

4.2 System Model

We consider a multi-hop NLOS UV system with M relay nodes as illustrated in Fig. 12. Let $m \rightarrow m+1$, $m = 0, ..., M$ denote the link between the m^{th} node and the $(m+1)^{\text{th}}$ node with a separation of $d_{m,m+1}$. The end-to-end distance i.e., distance between source (S) and destination (D) nodes is given by $d_{0,M+1}$. A detailed illustration of link $m \rightarrow m+1$ is given in Fig. 13. Transmitter at the m^{th} node emits a beam with divergence θ_{TX_m} and elevation angle β_{TX_m}. Receiver at the $(m+1)^{\text{th}}$ node has a field of view (FOV) of $\theta_{\text{RX}_{m+1}}$ and elevation angle of $\beta_{\text{RX}_{m+1}}$. In Fig. 13, V_m denotes the common volume for the link between the m^{th} node and

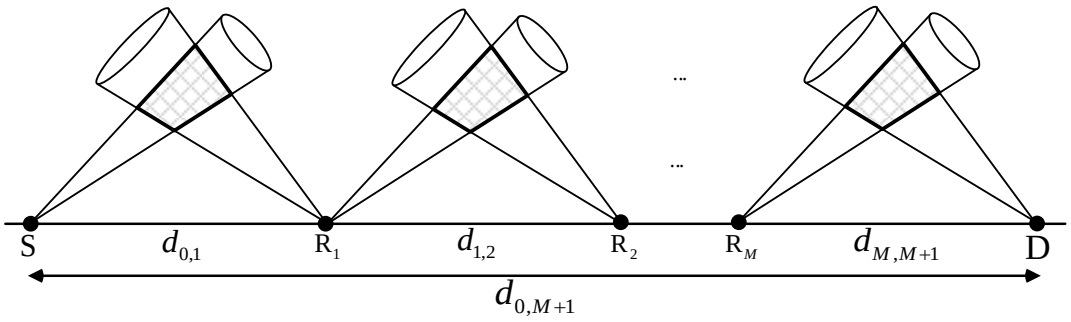

Figure 12: NLOS DF multi-hop configuration with M relay nodes.

the $(m+1)^{\text{th}}$ node. $d_{1-m,m+1}$ and $d_{2-m,m+1}$ respectively are the distance from the transmitter to V_m and from V_m to the receiver. They can be calculated in terms of the link distance $d_{m,m+1}$ as $d_{1-m,m+1} = d_{m,m+1}\sin\left(\beta_{\text{RX}_{m+1}}\right) / \sin\left(\theta_{\text{S}_{m,m+1}}\right)$ and $d_{2-m,m+1} = d_{m,m+1}\sin\left(\beta_{\text{TX}_m}\right) / \sin\left(\theta_{\text{S}_{m,m+1}}\right)$ where $\theta_{\text{S}_{m,m+1}} = \beta_{\text{TX}_m} + \beta_{\text{RX}_{m+1}}$.

We consider intensity-modulation direct-detection (IM/DD) with binary pulse position modulation (BPPM). In multi-hop system with DF relaying, the source node transmits a signal to an adjacent relay node. The relay retrieves the message signal, modulates it and retransmits it to the next hop only if the received SNR exceeds a given threshold to avoid error propagation. This continues until the source data arrives at the destination node.

Assume that P_t is the total power budget. Each node in the multi-hop system is assigned a transmit power of $P = P_t/(M+1)$. The received signals at the $(m+1)^{\text{th}}$node corresponding to the signal and non-signal slots of BPPM pulse are given by

$$r_{m+1} = \begin{cases} RTPg_{m,m+1} + v_{m+1}, & \text{for signal slot} \\ v_{m+1}, & \text{for non} - \text{signal slot} \end{cases} \tag{45}$$

where R is the receiver responsivity, T is the half bit interval, and v_{m+1} is signal-independent AWGN term with zero mean and variance $N_0/2$. In (45), $g_{m,m+1} =$

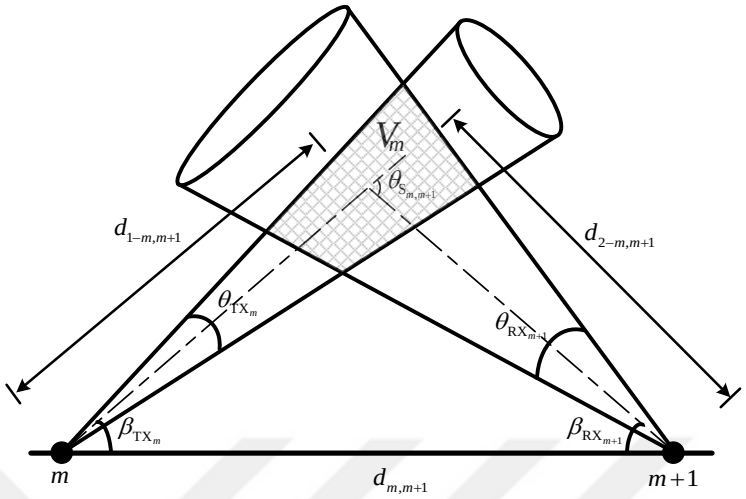

Figure 13: Detailed illustration of link $m \to m+1$.

$\alpha_{m,m+1}L_{m,m+1}$ denotes the channel coefficient for link $m \to m+1$ where $\alpha_{m,m+1}$ denotes the fading coefficient and it follows an log-normal PDF (see Chapter 2-Section 2.3) as

$$f\left(\alpha_{m,m+1}\right) = \frac{1}{\sqrt{2\pi}\sigma_{\mathrm{NLOS}_{m,m+1}}\alpha_{m,m+1}} \exp\left(-\frac{\left(\ln\left(\alpha_{m,m+1}\right) + \mu_{\mathrm{NLOS}_{m,m+1}}\right)^2}{2\sigma^2_{\mathrm{NLOS}_{m,m+1}}}\right), \quad (46)$$

where $\sigma^2_{\mathrm{NLOS}_{m,m+1}} = \sigma^2_{d^{\mathrm{tx}}_{m,m+1}} + \sigma^2_{d^{\mathrm{rx}}_{m,m+1}}$, $\mu_{\mathrm{NLOS}_{m,m+1}} = 0.5\sigma^2_{\mathrm{NLOS}_{m,m+1}}$. It should be noted that the turbulence log amplitude variance for LOS channels is typically smaller than 0.3 under weak turbulence conditions [29]. This indicates that the turbulence power variance should be smaller than 1.2.

We further define the normalized attenuation as $L_{m,m+1} = \ell\left(d_{m,m+1}\right) \,/\, \ell\left(d_{0,M+1}\right)$, i.e., normalized with respect to the attenuation of direct link (S $\to$ D).The attenuation for link $m \to m+1$ can be expressed as $\ell_{m,m+1} = \ell^{\mathrm{t}}_{m,m+1}\ell^{\mathrm{s}}_{m,m+1}$ where $\ell^{\mathrm{s}}_{m,m+1}$ is attenuation due to scattering (c.f. (6)) . $\ell^{\mathrm{t}}_{m,m+1} = 10^{-a_{m,m+1}\,/\,10}$ is turbulence induced attenuation where $a_{m,m+1} = 2\sqrt{23.17C_n^2k^{7/6}}\left(\sqrt{d^{11/6}_{1-m,m+1}} + \sqrt{d^{11/6}_{2-m,m+1}}\right)$.

4.3 Outage Analysis and Diversity Gain

In this section, we first derive the outage probability of multi-hop UV system over NLOS log-normal turbulence channels. Then, based on the derived outage expressions, we analyze the diversity gains.

4.3.1 Outage Probability

Outage probability is defined as the probability that instantaneous received electrical SNR γ falls below threshold SNR γ_{th}. If γ exceeds γ_{th}, no outage happens and signal can be decoded with arbitrarily error probability. The instantaneous electrical received SNR for link $m \to m+1$ is given by $\gamma_{m,m+1} = \left(RTPg_{m,m+1}\right)^2 / N_0$. The outage probability for this intermediate link can be calculated as

$$\begin{aligned} P_{\text{out}}^{m,m+1} &= \Pr\left(\gamma_{m,m+1} < \gamma_{\text{th}}\right) \\ &= \Pr\left(\alpha_{m,m+1} < \tfrac{M+1}{L_{m,m+1}} \tfrac{P_{\text{th}}}{P_{\text{T}}}\right) \end{aligned} \tag{47}$$

where P_{th} denotes a threshold transmit power required to guarantee that no outage happens in a direct fading-free transmission from the source to the destination. The ratio $P_{\text{M}} = P_t / \,.P_{\text{th}}$ is sometimes referred to as "power margin" [36]. The outage probability for link $m \to m+1$ can be then written using the cumulative distribution function (CDF) of the log-normal distribution as

$$P_{\text{out}}^{m,m+1} = Q\left(\frac{\ln\left(L_{m,m+1} P_{\text{M}} / \,.(M+1)\right) + \mu_{\text{NLOS}_{m,m+1}}}{\sigma_{\text{NLOS}_{m,m+1}}}\right), \tag{48}$$

Similarly for S $\to$ D link, we have

$$P_{\text{out}}^{0,M+1} = Q\left(\frac{\ln\left(P_{\text{M}}\right) + \mu_{\text{NLOS}_{0,M+1}}}{\sigma_{\text{NLOS}_{0,M+1}}}\right). \tag{49}$$

In multi-hop DF relaying, outage of each intermediate hop may lead to the overall outage. The overall outage can be then written in terms of the outage probability of each individual link, i.e., $P_{\text{out}} = 1 - \prod_{m=0}^{M}\left(1 - P_{\text{out}}^{m,m+1}\right)$. This yields

$$P_{\text{out}} = 1 - \prod_{m=0}^{M} \left(1 - Q\left(\frac{\ln\left(L_{m,m+1} P_{\text{M}} / \,.(M+1)\right) + \mu_{\text{NLOS}_{m,m+1}}}{\sigma_{\text{NLOS}_{m,m+1}}}\right)\right). \tag{50}$$

4.3.2 Diversity Analysis

Diversity order is conventionally defined as the negative asymptotic slope of the error rate performance or outage probability versus SNR on a log–log scale. However, over log-normal fading channels, this conventional definition yields infinity and does not provide a meaningful measure for diversity order. In [37], the so-called *relative diversity order (RDO)* is introduced. RDO is a normalized diversity order with respect to the diversity gain of a benchmarking scheme (typically direct link for a multi-hop configuration). It is defined as

$$\text{RDO}\left(P_{\text{M}}\right) = \frac{\partial \ln P_{\text{out}} / \partial \ln P_{\text{M}}}{\partial \ln P_{\text{out}}^{0,M+1} \Big/ \partial \ln P_{\text{M}}}. \tag{51}$$

Replacing (49) and (50) in (51) and neglecting the higher order terms after expanding the numerator, we have

$$\text{RDO}\left(P_{\text{M}}\right) \approx \frac{\sum_{m=0}^{M} Q\left(A_{m,m+1}\right)\left(\partial \ln Q\left(A_{m,m+1}\right) / \partial \ln P_{\text{M}}\right)}{\left(\partial \ln Q\left(A_{0,M+1}\right) / \partial \ln P_{\text{M}}\right) \sum_{m=0}^{M} Q\left(A_{m,m+1}\right)}, \tag{52}$$

where $A_{m,m+1} = \left(\ln\left(P_{\text{M}}\right) + \ln\left(L_{m,m+1} / \left(M+1\right)\right) + \mu_{\text{NLOS}_{m,m+1}}\right) / \sigma_{\text{NLOS}_{m,m+1}}$ and $A_{0,M+1} = \left(\ln\left(P_{\text{M}}\right) + \mu_{\text{NLOS}_{0,M+1}}\right) / \sigma_{\text{NLOS}_{0,M+1}}$. Applying well known bounds on the Q-function [38] in (52), we have approximate upper and lower bounds as

$$\text{RDO}\left(P_{\text{M}}\right) \tilde{\leq} \frac{\sum_{m=0}^{M} \left(\frac{A_{m,m+1}}{\sigma_{\text{NLOS}_{m,m+1}}} + \frac{1}{A_{m,m+1}}\right) \frac{1}{A_{m,m+1}} \exp\left(-\frac{A_{m,m+1}^2}{2}\right)}{\left(\frac{A_{0,M+1}}{\sigma_{\text{NLOS}_{0,M+1}}} + \frac{A_{0,M+1}^2 - 1}{A_{0,M+1}\left(A_{0,M+1}^2 + 1\right)}\right) \sum_{m=0}^{M} \frac{A_{m,m+1}}{1 + A_{m,m+1}^2} \exp\left(-\frac{A_{m,m+1}^2}{2}\right)}, \tag{53}$$

$$\text{RDO}\left(P_{\text{M}}\right) \tilde{\geq} \frac{\sum_{m=0}^{M} \left(\frac{A_{m,m+1}}{\sigma_{\text{NLOS}_{m,m+1}}} + \frac{A_{m,m+1}^2 - 1}{A_{m,m+1}\left(A_{m,m+1}^2 + 1\right)}\right) \frac{A_{m,m+1}}{1 + A_{m,m+1}^2} \exp\left(-\frac{A_{m,m+1}^2}{2}\right)}{\left(\frac{A_{0,M+1}}{\sigma_{\text{NLOS}_{0,M+1}}} + \frac{1}{A_{0,M+1}}\right) \sum_{m=0}^{M} \frac{1}{A_{m,m+1}} \exp\left(-\frac{A_{m,m+1}^2}{2}\right)}. \tag{54}$$

The asymptotic RDO (ARDO) can be calculated by taking limits of (53) and (54) when $P_{\mathrm{M}} \to \infty$ and using squeezing theorem. Specifically, we obtain

$$\mathrm{ARDO} = \lim_{P_{\mathrm{M}} \to \infty} \frac{\sigma^2_{\mathrm{NLOS}_{0,M+1}} \sum_{m=0}^{M} \frac{1}{\sigma_{\mathrm{NLOS}_{m,m+1}}} \exp\left(-\frac{(\ln(P_{\mathrm{M}}))^2}{2\sigma^2_{\mathrm{NLOS}_{m,m+1}}}\right)}{\sum_{m=0}^{M} \sigma_{\mathrm{NLOS}_{m.m+1}} \exp\left(-\frac{(\ln(P_{\mathrm{M}}))^2}{2\sigma^2_{\mathrm{NLOS}_{m.m+1}}}\right)}. \tag{55}$$

Considering dominant terms of (55) as$P_{\mathrm{M}} \to \infty$, we have

$$\mathrm{ARDO} = \frac{\sigma^2_{\mathrm{NLOS}_{0,M+1}}}{\max\left[\sigma^2_{\mathrm{NLOS}_{m,m+1}}\right]} = \frac{d^{11/6}_{0,M+1}\left(\frac{\sin\left(\beta_{\mathrm{T}_0}\right)^{11/6} + \sin\left(\beta_{\mathrm{R}_{M+1}}\right)^{11/6}}{\sin(\beta_{\mathrm{T}_0} + \beta_{\mathrm{R}_{M+1}})^{11/6}}\right)}{\max\left[d^{11/6}_{m,m+1}\left(\frac{\sin(\beta_{\mathrm{T}_m})^{11/6} + \sin\left(\beta_{\mathrm{R}_{m+1}}\right)^{11/6}}{\sin(\beta_{\mathrm{T}_m} + \beta_{\mathrm{R}_{m+1}})^{11/6}}\right)\right]}. \tag{56}$$

As seen from (56), the value of ARDO depends on the system parameters such as elevation angles, i.e., $\beta_{\mathrm{TX}_0}, \beta_{\mathrm{RX}_{M+1}}, \beta_{\mathrm{TX}_m}, \beta_{\mathrm{RX}_{m+1}}$and distances $d_{0,M+1}$, $d_{m,m+1}$. In the following we consider two special cases and obtain the corresponding ARDO values.

Special Case I: Assume that relays are located equidistant from each other with a separation of $d_{m,m+1} = d_{0,M+1}/\,.(M+1)$. Furthermore assume that transmitter and receiver of S and D nodes have same elevation angles, i.e., $\beta_{\mathrm{TX}_0} = \beta_{\mathrm{RX}_{M+1}} = \beta$ and the elevation angles of transmitter and receivers of all other intermediate nodes are the same, i.e., $\beta_{\mathrm{TX}_m} = \beta_{\mathrm{RX}_m} = \beta'$. In this case ARDO in (56) reduces to

$$\mathrm{ARDO} = \frac{\sigma^2_{\mathrm{NLOS}_{0,M+1}}}{\max\left[\sigma^2_{\mathrm{NLOS}_{m,m+1}}\right]} = \Omega\,(M+1)^{11/6}, \tag{57}$$

In (56), $\Omega = 2\sin(\beta+\beta')^{11/6} \Big/ \left((2\cos(\beta))^{11/6}\left(\sin(\beta)^{11/6} + \sin(\beta')^{11/6}\right)\right)$for $M = 1$ and

$$\Omega = \begin{cases} 2\sin(\beta+\beta')^{11/6} \Big/ \left((2\cos(\beta))^{11/6}\left(\sin(\beta)^{11/6} + \sin(\beta')^{11/6}\right)\right) & \text{for } \Delta_1 > \Delta_2 \\ (\cos(\beta')/\cos(\beta))^{11/6} & \text{for } \Delta_1 < \Delta_2 \end{cases}. \tag{58}$$

for $M > 1$ where $\Delta_1 = \left(\sin(\beta)^{11/6} + \sin(\beta')^{11/6}\right) \Big/ \sin(\beta+\beta')^{11/6}$ and $\Delta_2 = 2\sin(\beta')^{11/6} \Big/ \sin(2\beta')^{11/6}$. It is interesting to note that with proper choice of elevation angels, Ω can take values higher than 1 which leads to an ARDO higher

than $(M+1)^{11/6}$. This means that in NLOS transmission we can obtain diversity orders higher than those achievable in LOS links.

Special Case II: Again assume that relays are located equidistant from each other i.e.,$d_{m,m+1} = d_{0,M+1}/\ .(M+1)$. Furthermore, assume that all transmitters and receivers have same elevation angles, i.e., $\beta_{\mathrm{TX}_m} = \beta_{\mathrm{TX}}$ and $\beta_{\mathrm{RX}_m} = \beta_{\mathrm{RX}}$ for all m. In this case ARDO reduces to

$$\mathrm{ARDO} = (M+1)^{11/6}\,. \tag{59}$$

This corresponds to the ARDO for IR LOS links reported earlier in [39].

4.4 Numerical Results and Discussions

In this section, we present numerical results along with Monte Carlo simulations to confirm the accuracy of our derivations. Unless otherwise stated, we assume $k_{\mathrm{s}} = 0.55\ \mathrm{km}^{-1}$, $k_{\mathrm{e}} = 1.352\ \mathrm{km}^{-1}$, $C_n^2 = 5 \times 10^{-15}\ \mathrm{m}^{-2/3}$ $\lambda = 260$ nm , $A_{\mathrm{R}} = 1.77\ \mathrm{cm}^2$,$\theta_{\mathrm{TX}_0} = 8$mrd, $\theta_{\mathrm{RX}_{M+1}} = 45^{\circ}$, $\theta_{\mathrm{TX}_m} = 8$ mrd, $\theta_{\mathrm{RX}_{m+1}} = 45^{\circ}$, $\beta_{\mathrm{TX}_0} = 30^{\circ}$, $\beta_{\mathrm{RX}_{M+1}} = 30^{\circ}$ and $d_{0,M+1} = 1$ km. In all figures, $M = 0$ corresponds to direct transmission. To ensure fair comparison, the available transmit power budget is kept the same for all systems under consideration.

In Fig. 14, we illustrate the outage probability of multi-hop UV system under consideration for different number of relay nodes. As a benchmark, the outage performance of direct transmission, i.e., M=0 is included. We set the multi-hop configuration parameters such that it satisfies the Special Case I discussed in Section 4.3.2. In this case, relays are located equidistant with $\beta' = 70^{\circ}$. The derived analytical expression in (50) is in excellent agreement with simulation results confirming the accuracy of our derivation. It is also observed that performance gains are highly dependent on system configuration and increasing the number of relays does not necessarily improve the system performance. For example, when $M = 1$, relay-assisted

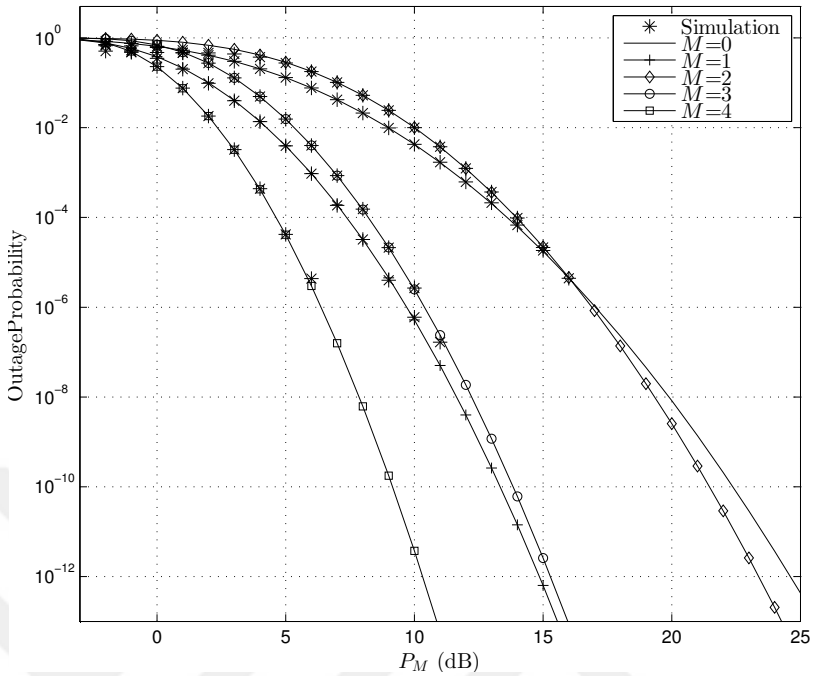

Figure 14: Outage probability of multi-hop UV system for different values of relay nodes ($\beta' = 70°$).

system significantly outperforms the direct transmission. Specifically, to achieve a target outage probability of 10^{-6}, SNR=17 dB is required for direct transmission while this decreases to 9.6 dB for a single-relay system indicating a performance gain of 7.4 dB. Interestingly, this gain vanishes for $M = 2$ and relay-assisted system is able to slightly outperform direct transmission only in high SNR values.

The observations from Fig.14 clearly indicate an irregular performance trend for relay-assisted UV systems. Note that for $M = 1$, we have only $\mathrm{S} \rightarrow \mathrm{R}_1$ and $\mathrm{R}_1 \rightarrow \mathrm{D}$ links with elevation angle pairs of $(30°, 70°)$ and $(70°, 30°)$ respectively. For $M = 2$, we have $\mathrm{R}_1 \rightarrow \mathrm{R}_2$ link with elevation angle pair of $(70°, 70°)$. Such a link has more path loss and experiences higher turbulence variance with respect to elevation angle pairs of $(30°, 70°)$ and $(70°, 30°)$. Adding more than one relay obviously decreases the separation distance between two consequence nodes. However, since the available transmit power budget is divided by the number of nodes, the transmit power may

not be sufficient to overcome the high path loss and turbulence of the links with high elevation angles. Therefore, such links become the bottleneck for the overall performance. When the number of relay nodes is further increased (see $M = 4$ in Fig.14), the separation distance decreases to an extent where the degradations associated with path loss and turbulence are less than the transmit power decrement. This therefore reverses the performance trend.

In Fig. 15, we depict the RDO for the multi-hop UV systems considered in Fig. 14. ARDO values derived in (57) are also plotted. We consider $P_{\mathrm{M}} = 400$ dB (chosen very large for the purpose of asymptotical analysis) and observe ARDO values of 2.158, 1.365, 2.312 and 3.514 respectively for $M = 1$, 2, 3 and 4. These coincide to the derived ARDOs in (57) which yields $\Omega\,(M+1)^{11/6} = 2.158$, 1.365, 2.312 and 3.481. The outage performance trends observed in Fig. 14 can be also seen here. The ARDO for $M = 2$ is less than that of $M = 1$. The RDO for $M = 2$ in low P_{M} takes values even less than one indicating no gain with respect to the direct transmission. At higher P_{M} values, it converges to ARDO=1.365, but still remains smaller than the ARDO=2.158 achieved by $M = 1$. It can be seen that in low SNR regime for $M = 3$, the RDO values are less than those of $M = 1$. However in high SNR values they converge to ARDO=2.312 which is slightly better than that of $M = 1$. For $M = 4$, the RDO values are always better than $M = 1$ for all SNR values.

It was observed from Figs. 14 and 15 that increase in the number of relays does not necessarily improve the performance and particularly the elevation angles significantly affect the overall performance. To provide a better insight, we investigate the outage performance with respect to relay nodes elevation angles. In Fig. 16, we assume a fixed SNR of 8 dB, consider $M = 1,\ 2,\ ...,\ 6$ and assume that the elevation angles of transmitter and receivers of all other intermediate nodes are the same, i.e., $\beta_{\mathrm{TX}_m} = \beta_{\mathrm{RX}_m} = \beta'$. It is observed that a single-relay system outperforms direct transmission for all β' values under consideration. On the other hand, for high β' values, the

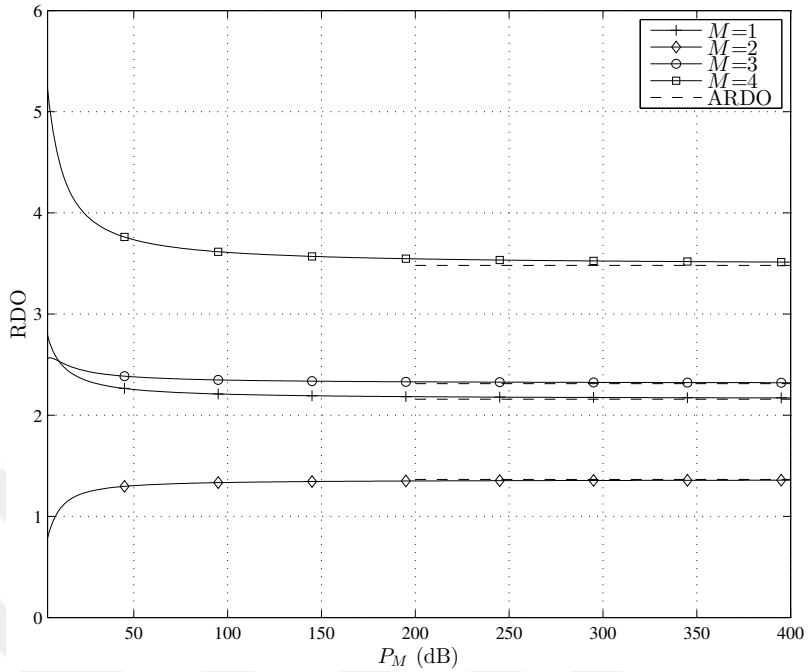

Figure 15: RDO for different values of relay numbers.

performance of direct transmission might be better than the performance of a relay-assisted system with more than one relay. There is actually a specific threshold for β' to ensure gains over direct transmission. It is observed from Fig.16 that for $M = 2$, the threshold elevation angle which guarantees better performance with respect to direct transmission is $\beta' = 68°$. This increases to $\beta' = 73°, 76°, 78°, 79°$ for $M = 3,\ 4,\ 5,\ 6$ respectively.

In Fig. 17, we assume that relays are located equidistant with sufficiently small elevation angles (i.e., $\beta' = 30^{\circ}$) and illustrate the outage probability of multi-hop UV system for $M = 1,\ 2,\ 3, 4$. These assumptions satisfy the Special Case II discussed in Section 4.3.2. Unlike Fig.14, we now observe a consistent performance improvement when the number of relays increases. Particularly, to achieve a target outage probability of 10^{-6}, only SNR=2 dB is required for $M = 1$ indicating a performance gain of 15 dB over direct transmission. This significant performance gain further increases to 21 dB, 24 dB and 26.2 dB for $M = 2,\ 3$ and 4, respectively. In Fig. 18, we depict

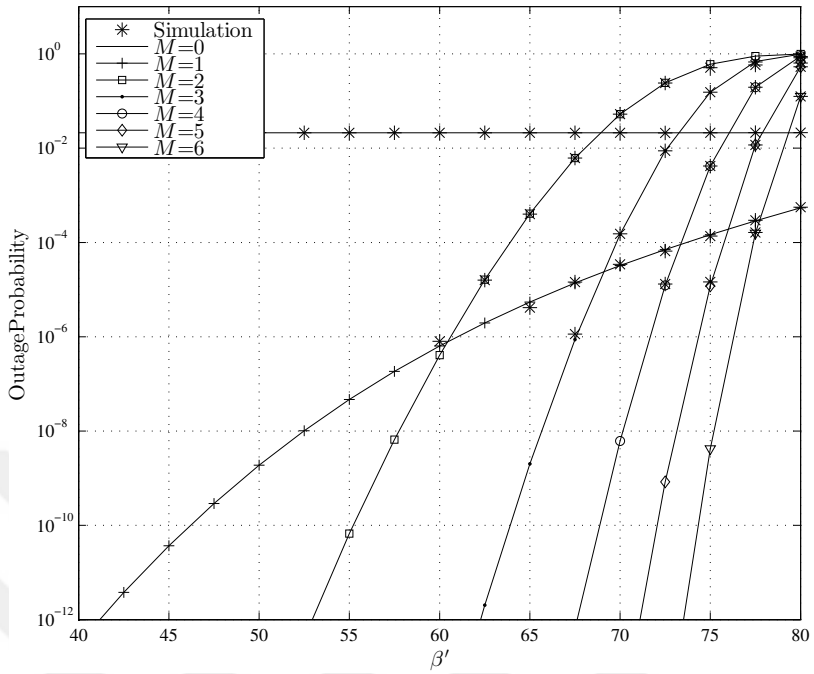

Figure 16: Outage probability for different values of elevation angles (β').

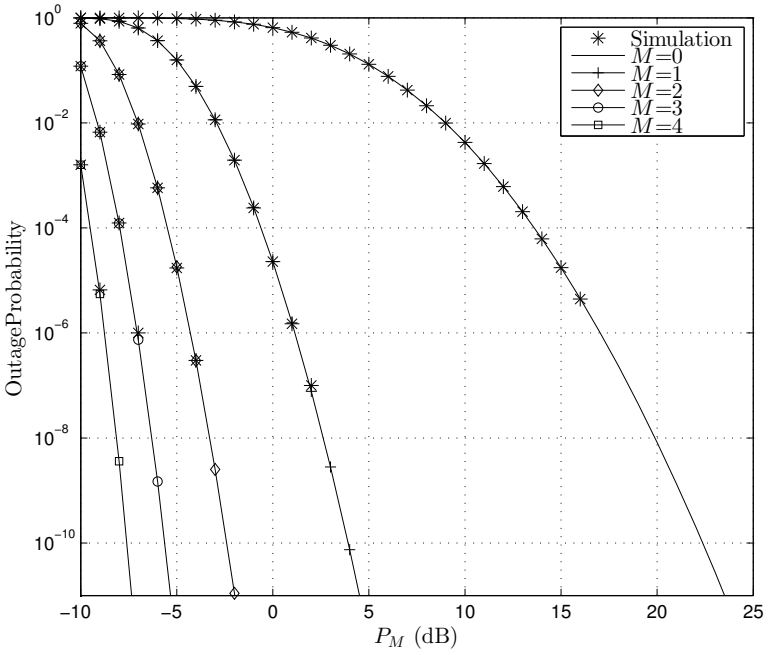

Figure 17: Outage probability of multi-hop UV system for different values of relay nodes ($\beta' = 30°$).

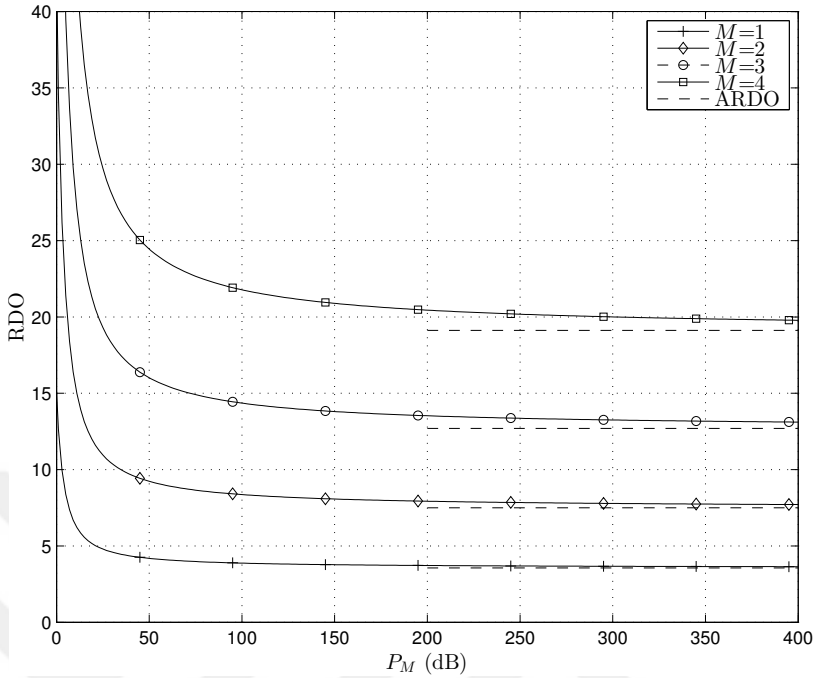

Figure 18: RDO for different values of relay numbers (Special Case II).

the diversity gains for the systems considered in Fig. 17. We observe ARDO values of 3.641, 7.711, 13.11 and 19.78 respectively for $M = 1$, 2, 3 and 4. These coincide to the derived ARDOs in (59) which yield $(M+1)^{11/6} = 3.564$, 7.494, 12.700 and 19.120.

In Fig. 19, we consider a multi-hop system with $M = 3$ where relays are located equidistant from each other. We assume $\left(\beta_{\mathrm{TX}_0}, \beta_{\mathrm{RX}_{M+1}}\right) = \left(45^\circ,\ 45^\circ\right)$ at the source and destination while we consider several values for relay nodes elevation angles which are assumed to be equal to each other, i.e., $\beta_{\mathrm{TX}_m} = \beta_{\mathrm{RX}_m} = \beta'$. This assumption satisfies the Special Case I discussed in Section IV.b. For $P_{\mathrm{M}} = 400$ dB, we observe ARDO values of 11.06 and 6.944 for $\beta' = 50^\circ$ and 60° respectively. These are lower than 12.699 which is the ARDO value for LOS link obtained from (59). On the other hand, for $\beta' = 20^\circ,\ 30^\circ$, ARDOs are calculated as 17.58 and 16.27 respectively which exceed those in LOS links. This confirms our earlier observation that when the elevation angle gets smaller (which satisfies the condition of $\Delta_1 > \Delta_2$ in Section 4.3.2), it is possible to achieve ARDOs higher than those in LOS links.

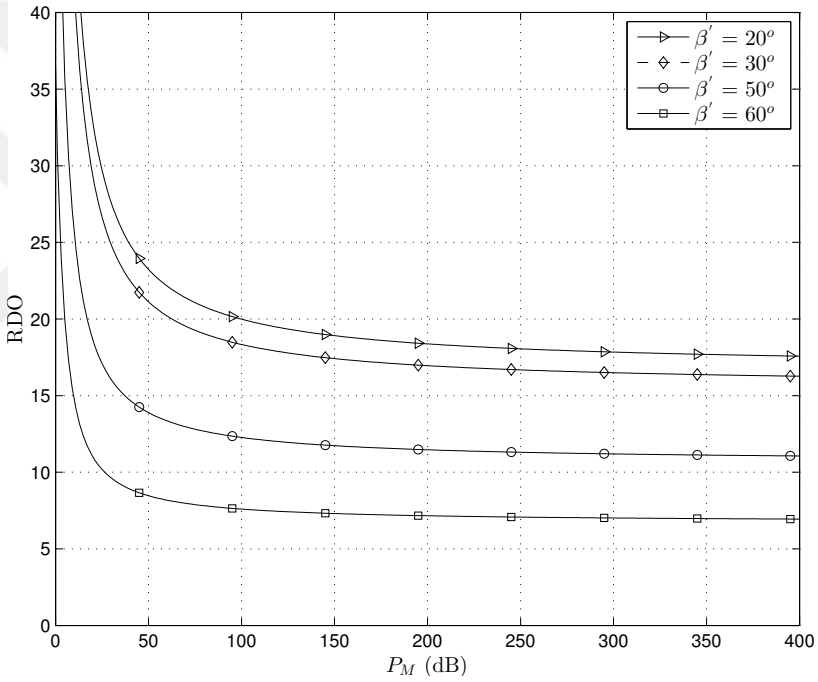

Figure 19: RDO for different values of elevation angles (Special Case I).

CHAPTER V

MIMO NLOS UV COMMUNICATIONS

5.1 Introduction

In the previous chapters, we investigated relay-assisted systems that can be considered as distributed spatial diversity system. The employment of co-located multiple transmitters/receivers can also improve link reliability (through diversity gain) or throughput rate (through multiplexing gain). In this chapter, we consider MIMO UV systems and investigate their performance over turbulence channels.

5.2 System and Channel Model

Fig.20.a. illustrates MIMO NLOS UV link with M transmitters and N receivers under consideration. The link distance is denoted by d . The detailed illustration of link between the m^{th} transmitter and the n^{th} receiver is provided in Fig 23.b. The m^{th} transmitter emits a beam with divergence $\theta_{\text{TX},m}$ and elevation angle $\beta_{\text{TX},m}$. The n^{th} receiver has a field of view (FOV) of $\theta_{\text{RX},n}$ and elevation angle of $\beta_{\text{RX},n}$. The common volume between the m^{th} transmitter and the n^{th} receiver is denoted by V_{mn}. $d_{1,mn}$ and $d_{2,mn}$ respectively denote the distance from the m^{th} receiver to V_{mn} and from V_{mn} to the n^{th} receiver. They can be calculated in terms of d as $d_{1,mn} = d\sin(\beta_{RX,n}) \,/\, \sin(\theta_{\text{s},mn})$ and $d_{2,mn} = d\sin(\beta_{\text{TX},m}) \,/\, \sin(\theta_{\text{s},mn})$ where $\theta_{\text{s},mn} = \beta_{\text{TX},m} + \beta_{\text{RX},n}$.

We employ on-off keying (OOK) with intensity modulation and direct detection (IM/DD). We assume perfect channel state information (CSI) at the receiver side. The received signal at the n^{th}receiver is given by

$$r_n = \sum_{m=1}^{M} \eta P_{t,m} I_{r,mn} x + v_n;\ n = 1,\ 2,\ ..., N \tag{60}$$

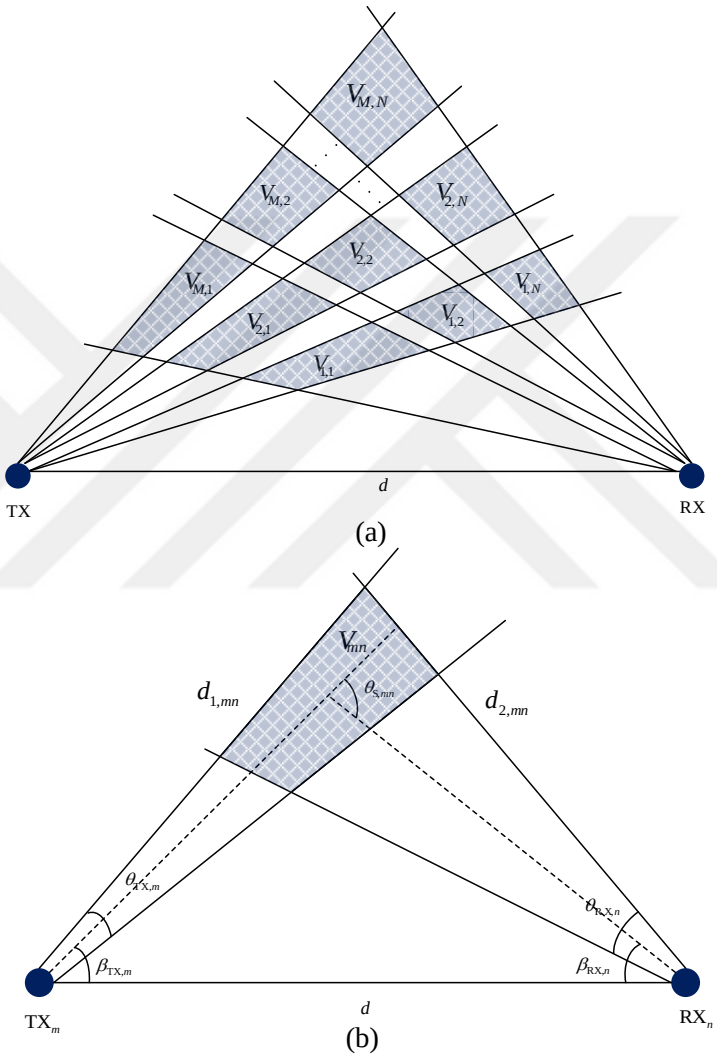

Figure 20: (a) NLOS MIMO UV system under consideration (b) Detailed illustration of the link between the m^{th} transmitter (TX_m) and the n^{th} receiver (RX_n).

where $x \in [0,1]$ denotes information bit, η is the optical-to-electrical conversion coefficient and $P_{t,m}$ is the optical transmit power emitted from the m^{th} transmitter. v_n is the signal independent AWGN with zero mean and variance $\sigma_v^2 = N_0 / .2$.

In (60), $I_{r,mn}$ denotes the received optical power between the m^{th} transmitter and the n^{th} receiver including both path loss and turbulence effects which follows log-normal distribution as discussed in chapter 2 as

$$f\left(I_{r,mn}\right) = \frac{1}{\sqrt{2\pi}\sigma_{\text{mn}} I_{r,mn}} \exp\left(-\frac{1}{2\sigma_{\text{mn}}^2}\left(\ln\left(I_{r,mn}\right) - \mu_{\text{mn}}\right)^2\right). \tag{61}$$

In (61), $\sigma_{mn}^2 = 1.23 C_n^2 k^{7/6}\left(d_{1,mn}^{11/6} + d_{2,mn}^{11/6}\right)$ and $\mu_{mn} = -0.5\sigma_{mn}^2 - \alpha_{mn}\ln 10/10 + \ln\left(I_{0,mn}\right)$ where $\alpha_{mn} = 2\sqrt{23.17 C_n^2 k^{7/6}}\left(\sqrt{d_{1,mn}^{11/6}} + \sqrt{d_{2,mn}^{11/6}}\right)$. $I_{0,mn}$ corresponds to the received irradiance in the absence of turbulence under single scattering assumption for unit transmitter power and is given by

$$I_{0,mn} = \frac{k_s \Psi\left(\theta_{s,mn}\right) A_{\text{RX},n} \exp\left(-k_e\left(d_{1,mn} + d_{2,mn}\right)\right) V_{mn}}{2\pi\left[1 - \cos\left(\theta_{\text{TX,m}}/2\right)\right] d_{2,mn}^2 d_{1,mn}^2}. \tag{62}$$

Note that, parameters of PDF (i.e., σ_{mn}^2, α_{mn}, and $I_{0,mn}$) are functions of $d_{1,mn}$ and $d_{2,mn}$. Hence, except the case that all transmitters and receivers look at the same common volume (i.e., $\beta_{\text{TX},1} = \beta_{\text{TX},2} = ... = \beta_{\text{TX},M}$ and $\beta_{\text{RX},1} = \beta_{\text{RX},2} = ... = \beta_{\text{RX},N}$), the underlying links are non-identical fading. Furthermore, the non-correlation distance for UV wavelengths is in order of centimeters and is larger than $\sqrt{\lambda d}$. Therefore, we assume independent non identical fading channels in our work.

5.3 BER Performance in MIMO NLOS Link

The optimum decision metric for OOK is given by [15, eq. (16)]

$$P\left(.\mathbf{r}\middle| on, I_{mn}\right) \underset{off}{\overset{on}{\gtrless}} P\left(.\mathbf{r}\middle| off, I_{mn}\right), \tag{63}$$

where $\mathbf{r} = (r_1, r_2, ..., r_n)$ is the received signal vector. The conditional probabilities of the received vector being in "off" or in "on" state are respectively given by

$$P\left(\mathbf{r}\middle| off, I_{mn}\right) = \frac{1}{\left(2\pi\sigma_n^2\right)^{N/2}} \exp\left(-\frac{1}{2\sigma_n^2}\sum_{n=1}^{N} r_n^2\right), \tag{64}$$

$$P\left(\mathbf{r}|\, on, I_{mn}\right) = \frac{\exp\left(-\frac{\sum_{n=1}^{N}\left(r_n - \eta\sum_{m=1}^{M} P_{t,m} I_{mn}\right)^2}{2\sigma_n^2}\right)}{\left(2\pi\sigma_n^2\right)^{N/2}}. \tag{65}$$

Assuming equal probable messaging and following similar steps as in [15], the average BER is obtained as

$$P_{e,\mathrm{MIMO}} = \int_{\mathbf{I}} f_{\mathbf{I}}\left(\mathbf{I}\right) Q\left(\frac{1}{M}\frac{\eta P_t}{\sqrt{2N_0}}\sqrt{\sum_{n=1}^{N}\left(\sum_{m=1}^{M} I_{mn}\right)^2}\right) d\mathbf{I}, \tag{66}$$

where $Q\left(x\right) = \left(1/\ .\sqrt{2\pi}\right)\int_x^{\infty}\exp\left(-t^2/2\right)dt$ is the Gaussian Q-function. In (66), $f_{\mathbf{I}}\left(\mathbf{I}\right)$ is the joint PDF of vector $\mathbf{I} = \left(I_{11}, I_{12}, ..., I_{MN}\right)$ of length MN and the scaling factor of $1/M$ is used to keep the total power budget P_t the same as in SISO system. (66) can be calculated with the help of mathematical software packages through multi-dimensional numerical integration. To have further insight into the performance of UV links with spatial diversity, we investigate transmit and receive diversity as special cases.

5.3.1 MISO NLOS Link

When transmit diversity is considered i.e., $N = 1$, (66) reduces to

$$P_{e,\mathrm{MISO}} = \int_{\mathbf{I}} f_{\mathbf{I}}\left(\mathbf{I}\right) Q\left(\frac{1}{M}\frac{\eta P_t}{\sqrt{2N_0}}\sum_{m=1}^{M} I_{m1}\right) d\mathbf{I}, \tag{67}$$

which requires M-dimensional integral. To obtain a closed-form expression, we approximate the sum of independent log-normal distributed random variables as a single log-normal variable [40]. Specifically, we define $I_{\mathrm{MISO}} \approx \sum_{m=1}^{M} I_{m1}$. It can be shown that I_{MISO} follows log-normal distribution with mean μ_{MISO} and the variance of σ^2_{MISO} which are respectively given by

$$\mu_{\mathrm{MISO}} = \ln\left(\sum_{m=1}^{M} I_{0,m1} 10^{-\alpha_{m1}/\,.10}\right) - \frac{\sigma^2_{\mathrm{MISO}}}{2}, \tag{68}$$

$$\sigma^2_{\mathrm{MISO}} = \ln\left(1 + \frac{\sum_{m=1}^{M} I^2_{0,m1} 10^{-2\alpha_{m1}/\,.10}\left(e^{\sigma^2_{m1}} - 1\right)}{\left(\sum_{m=1}^{M} I_{0,m1} 10^{-\alpha_{m1}/\,.10}\right)^2}\right). \tag{69}$$

By using approximation of $e^{\sigma_{m1}^2}-1 \approx \sigma_{m1}^2$ for small σ_{m1}^2, (69) can be further simplified as

$$\sigma_{\text{MISO}}^2 \approx \ln\left(1+\frac{\sum_{m=1}^{M} I_{0,m1}^2 10^{-2\alpha_{m1}/10}\sigma_{m1}^2}{\left(\sum_{m=1}^{M} I_{0,m1}10^{-\alpha_{m1}/10}\right)^2}\right) \approx \frac{\sum_{m=1}^{M} I_{0,m1}^2 10^{-2\alpha_{m1}/10}\sigma_{m1}^2}{\left(\sum_{m=1}^{M} I_{0,m1}10^{-\alpha_{m1}/10}\right)^2}, \tag{70}$$

where the second approximation in (70) comes from $\ln(1+z) \approx z$ for small z. For a sanity check, assume that all transmitter and receiver pairs have the same set of configurations, i.e., $\sigma_{m1}^2 = \sigma^2$, $\alpha_{m1} = \alpha$, $I_{0,m1} = I_0$ which leads to identical fading distribution. Therefore (70) reduces to $\sigma_{\text{MISO}}^2 = \sigma^2/M$. A similar result has been earlier reported in the context of IR LOS links [15]. This shows that the fading variance is scaled by the number of transmitters.

Replacing I_{MISO} in (67), we have

$$P_{e,\text{MISO}} \approx \int_0^\infty f_{I_{\text{MISO}}}(I_{\text{MISO}})\, Q\left(\frac{1}{M}\frac{\eta P_t}{\sqrt{2N_0}} I_{\text{MISO}}\right) dI_{\text{MISO}}, \tag{71}$$

which is one-dimensional integration similar to SISO transmission. Integration in (71) can be efficiently approximated by Gauss-Hermite quadrature formula [37]

$$P_{e,\text{MISO}} \approx \frac{1}{\sqrt{\pi}} \sum_{i=1}^{k} w_i Q\left(\frac{\eta P_t}{M\sqrt{2N_0}} e^{z_i\sqrt{2\sigma_{\text{MISO}}^2}+\mu_{\text{MISO}}}\right), \tag{72}$$

where w_i and z_i , $i = 1,\ 2,\ ...,\ k$ are respectively weight factors and the zeroes of the k^{th} order Hermite polynomial.

5.3.2 SIMO NLOS Link

Consider receive diversity with maximal ratio combining (MRC). Replacing $M = 1$ in (66), we have

$$P_{e,\text{SIMO}} = \int_{\mathbf{I}} f_{\mathbf{I}}(\mathbf{I})\, Q\left(\frac{\eta P_t}{\sqrt{2N_0}}\sqrt{\sum_{n=1}^{N} I_{1n}^2}\right) d\mathbf{I}, \tag{73}$$

which requires N-dimensional integral. Note that I_{1n}^2 follows log-normal distribution with mean $2\mu_{1n}$ and $4\sigma_{1n}^2$. As in Section 5.3.1, the sum of log-normal random variables can be approximated with another log-normal random variable. Hence we can write $I_{\text{SIMO}} \approx \sum_{n=1}^{N} I_{1n}^2$. Similar to I_{MISO}, I_{SIMO} follows log-normal distribution with mean μ_{SIMO} and the variance of σ_{SIMO}^2. Its mean and the variance can be calculated through (74) and (75) as

$$\mu_{\text{SIMO}} = \ln\left(\sum_{n=1}^{N} I_{0,1n}^2 10^{-2\alpha_{1n}/10} e^{\sigma_{1n}^2}\right) - \frac{\sigma_{\text{SIMO}}^2}{2}, \tag{74}$$

$$\sigma_{\text{SIMO}}^2 = \ln\left(1 + \frac{\sum_{n=1}^{N} I_{0,1n}^4 10^{-4\alpha_{1n}/10} e^{2\sigma_{1n}^2}\left(e^{4\sigma_{1n}^2} - 1\right)}{\left(\sum_{n=1}^{N} I_{0,1n}^2 10^{-2\alpha_{1n}/10} e^{\sigma_{1n}^2}\right)^2}\right). \tag{75}$$

Therefore (73) can be simplified to

$$P_{e,\text{SIMO}} \approx \int_0^{\infty} f_{I_{\text{SIMO}}}(I_{\text{SIMO}})\, Q\left(\frac{\eta P_t}{\sqrt{2N_0}}\sqrt{I_{\text{SIMO}}}\right) dI_{\text{SIMO}}, \tag{76}$$

which can be computed by single integration and approximated by Gauss-Hermite quadrature formula.

5.4 Numerical Results and Discussions

For the numerical study in this section, we assume $k_s^{Ray} = 0.266\,\text{km}^{-1}$, $k_s^{mie} = 0.284\,\text{km}^{-1}$, $k_{\text{e}} = 1.352\,\text{km}^{-1}$,$\lambda = 260\,\text{nm}$, $\alpha_{mn} = 0$, $A_{\text{RX}} = 1.77\,\text{cm}^2$ and set $(\theta_{\text{TX}},\, \theta_{\text{RX}}) = \left(3\text{mrd},\, 30^{\circ}\right)$ for all transmitters and receivers. In each set of configurations, the link between the first transmitter and the receiver is assumed to have the smallest elevation angle and less attenuation i.e., the link with best performance. We consider this SISO link as a benchmark. Therefore, in BER performance comparisons, we normalize the received irradiance in the absence of turbulence of each transmitter and receiver pairs to that of SISO link.

Fig. 21 illustrates the BER performance of a MISO UV link with two and three transmitters. As a benchmark, the BER performance of SISO link is also included.

We assume$(\beta_{\mathrm{TX},1}, \beta_{\mathrm{TX},2}, \beta_{\mathrm{TX},3}, \beta_{\mathrm{RX},1}) = (20^\circ, 21^\circ, 22^\circ, 30^\circ)$[1]. The approximate BER expressions in (71) are illustrated along with the exact expression (67) which requires multidimensional integrations. It is observed that they are in good agreement. Some discrepancy is observed for large distance links where the fading variance is larger. Our results demonstrate BER improvements through the deployment of multiple transmitters. For example, to achieve a target BER of 10^{-6} for $d = 1000$ m, an SNR of 36 dB is required for SISO link. This reduces to 33 dB and 32.5 dB for two and three transmitter respectively indicating performance gains of 3 and 3.5 dB. For $d = 500$ m, an SNR of 19 dB is required for SISO link. Performance gains of 1 dB are obtained for two and three transmitters. It is observed that the employment of third transmitter does not bring any further gain over the configuration with two transmitters. In general, particularly in the low to medium SNR regions, we can conclude that gains become either negligible or even non-existent. This is due to the fact that, to keep the power budget the same as in the SISO system, the transmit power for each transmitter is divided by a factor of M and the links with high elevation angles experience more attenuation and manifests its effect particularly in low to medium SNR regime.

Fig. 22 illustrates the BER performance of a SIMO UV link with two and three receivers. In this figure, we consider $(\beta_{\mathrm{RX},1}, \beta_{\mathrm{RX},2}, \beta_{\mathrm{RX},3}, \beta_{\mathrm{TX},1}) = (30^\circ, 50^\circ, 70^\circ, 20^\circ)$[1]. Similar to Fig. 21, the derived approximate expressions, i.e. (76) are in good agreement with exact ones (73). It is observed that adding more receivers improves the performance. Unlike the SIMO case discussed above, more gains are observed as the total received SNR further increases due to array gain [41]. As an example, to achieve a target BER of 10^{-6} for $d = 1000$ m, an SNR of 36 dB is required for SISO link. This reduces to 32 dB and 30.5 dB for two and three receivers respectively indicating

[1]Unlike [20] we consider a general system configuration and set the elevation angles of the transmitters/receivers such that they do not look at the same common volume

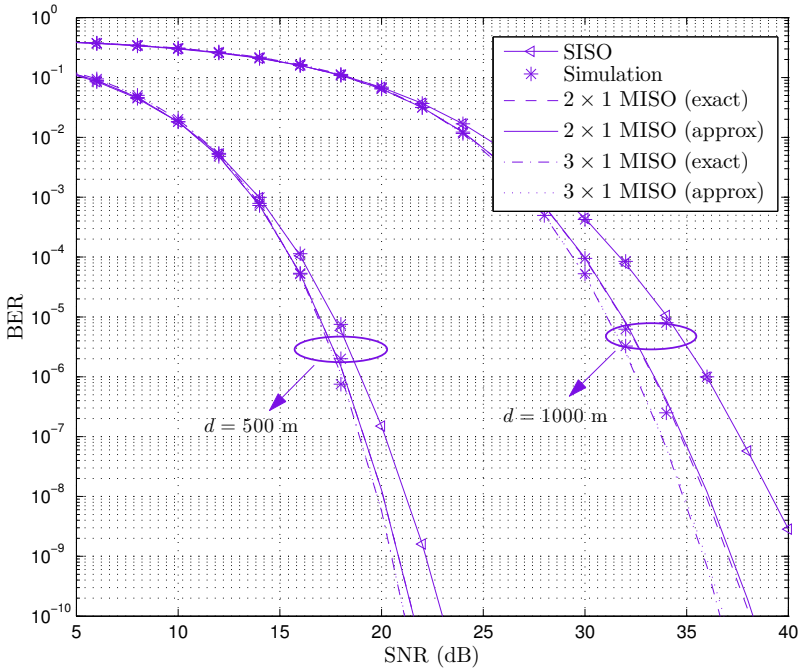

Figure 21: BER performance of MISO UV system for 2 and 3 transmitters.

performance gains of 4 dB and 5.5 dB. For $d = 500$ m, performance gains of 3 and 4 dB are obtained for two and three receivers respectively.

Fig. 23 illustrates the BER performance of 2×2 and 3×3 MIMO systems based on the expression in (66). In this figure, we consider $(\beta_{\mathrm{RX},1}, \beta_{\mathrm{RX},2}, \beta_{\mathrm{RX},3}) = (30°, 50°, 70°)$ and $(\beta_{\mathrm{TX},1}, \beta_{\mathrm{TX},2}, \beta_{\mathrm{TX},3}) = (20°, 21°, 22°)$. It should be noted that, as earlier mentioned for MISO systems illustrated in Fig. 24, adding more transmitters does not always lead in improvement of BER performance particularly in low SNR regime. For example, a 3×3 MIMO system with a link range of 500 m outperforms the 2×3 MIMO system only in high SNR. To further highlight this effect, in Fig. 24 we compare the performance of MISO and MIMO systems where the transmitters look at the same common volume. We consider $d = 1000$ $m$and same elevation angles of $\beta_{\mathrm{TX},i} = 20°$ $(i = 1,\ 2,\ 3)$ for transmitters and $(\beta_{\mathrm{RX},1}, \beta_{\mathrm{RX},2}, \beta_{\mathrm{RX},3}) = (30°, 50°, 70°)$ for receivers. As can be seen from the figure, as opposed to Fig. 21 adding more number of transmitters leads to better BER performance for all range of SNR values. This is

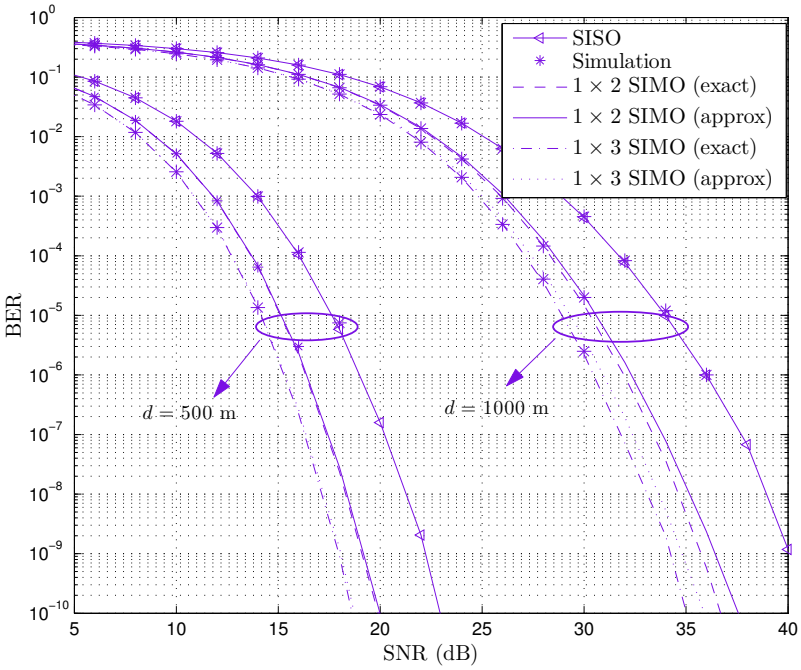

Figure 22: BER performance of SIMO UV system for 2 and 3 receivers.

due to the fact that all the links experience the same attenuation and average received power without turbulence is similar to the SISO case while the variance of the fading is divided by the factor of the number of transmitters. Similar behavior can be seen for MIMO system where 3×3MIMO system outperforms 2×3 MIMO system for all ranges of SNR.

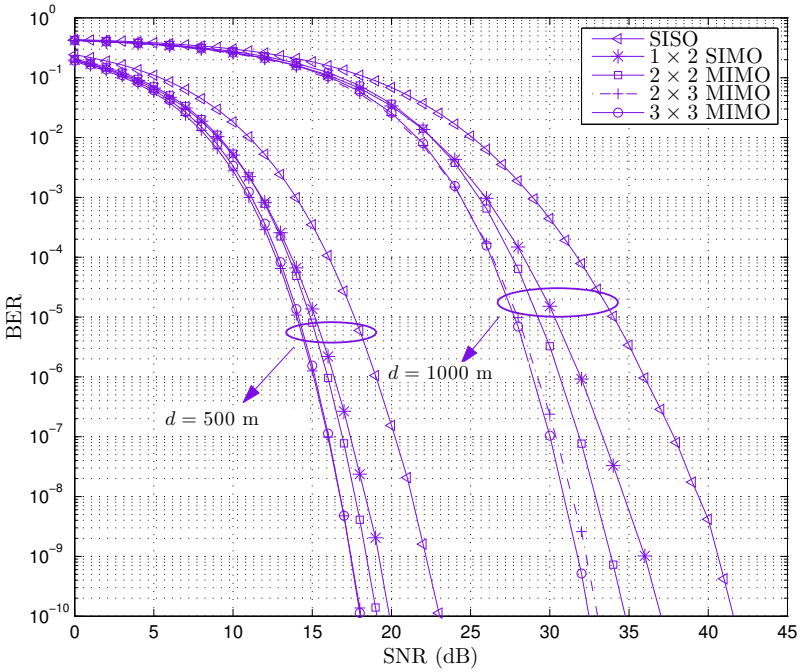

Figure 23: BER performance of MIMO systems.

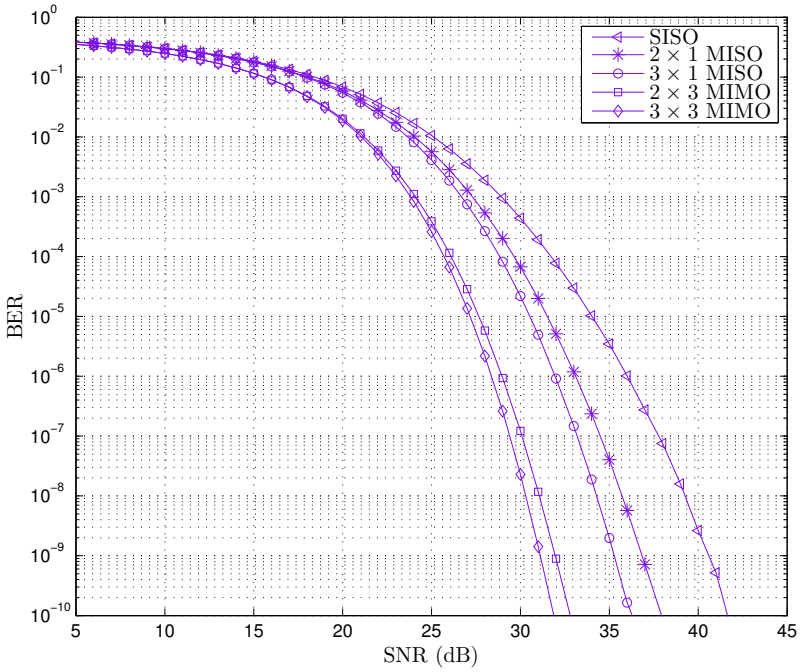

Figure 24: Performance comparison of MISO and MIMO UV systems.

CHAPTER VI

CONCLUSIONS

In this thesis, we investigate relay-assisted and MIMO communications in the context of NLOS UV communication.

In the first part, we have proposed the use of OFDM-based relay-assisted transmission for NLOS UV communication. Specifically, we have considered a three node DCO-OFDM system with orthogonal cooperation protocol and presented an extensive performance analysis and optimization. For both AF and DF relaying, we have derived approximate closed-form expressions for optimal AC and DC power allocation and verified them through numerical optimization. Our simulation results have shown that the performance of proposed cooperative transmission is highly dependent on relay location and system geometry. When the system configuration is symmetrical (i.e., links S $\rightarrow$ R and R $\rightarrow$ D have the same FOVs and elevation angles), a relay at midpoint between source and destination provides the highest performance gains over point-to-point transmission. If relay FOV is wider than destination FOV, a relay closer to destination becomes preferable. If relay transmitter has a smaller elevation angle, a relay closer to source is favorable. Our results further indicate that OPA is required in relay-assisted UV systems to realize gains over point-to-point transmission for most relay locations. Finally, we have investigated bit loading for a variable-rate cooperative UV system and demonstrated improvements in throughput.

In the second part of this thesis, we investigated the effects of turbulence on the performance of multi-hop NLOS UV systems. We have derived closed-form outage probability expressions and quantified the diversity gains as a function of system and channel parameters. Our results have interestingly demonstrated that increase

in the number of relays does not necessarily improve the performance and the overall performance is highly dependent on system configuration, particularly the elevation angles. We have observed that a singlerelay system outperforms direct transmission for all elevation angles values under consideration. For higher number of relay nodes, there exist some threshold values for elevation angles to ensure gain over direct transmission. Our results have further demonstrated that NLOS system can offer higher diversity gain compared to that of LOS system when relay nodes have smaller elevation angles than those of source and destination nodes.

In the third part, we have investigated the performance of MIMO NLOS UV communication systems over NLOS turbulence channels. Since the BER expressions for MIMO UV channels are in a multi-dimensional integral form, we have introduced approximate BER expressions through the approximation of sum of log-normal random variables. Simulation results are used to confirm the accuracy of our approximation. Analytical and simulation results reveal that multiple transmitters or receivers decreases the variance of the channel and therefore, significantly improves BER performance. However, it is observed that adding more transmitters does not always lead to the performance gain in low to moderate SNR regime. When the transmitters look at the same common volume, the performance gain is guaranteed for all SNR ranges.

APPENDIX A

PDF OF RECEIVED OPTICAL POWER IN A NLOS UV LINK

In this Appendix, we derive a closed-form expression for the PDF of received optical power in a NLOS UV link. The joint PDF of I_v and I_r is $.f\left(I_r, I_v\right) = f(I_r|I_v)f(I_v)$. Therefore, the PDF of the received optical power can be obtained by $f\left(I_r\right) = \int f(I_r|I_v)\, f\left(I_v\right) dI_v$ i.e.,

$$f\left(I_r\right) = \vartheta_1 \int_0^{\infty} \vartheta_2 dI_v, \tag{77}$$

where ϑ_1 and ϑ_2 are respectively defined as

$$\vartheta_1 = \frac{1}{I_r\sqrt{2\pi}\sigma_{d_1}\sigma_{d_2}} \exp\left(-\frac{\left(\ln I_r + \mu_2'\right)^2}{2\sigma_2^2} - \frac{{\mu_1'}^2}{2\sigma_{d_1}^2}\right), \tag{78}$$

$$\vartheta_2 = \frac{1}{\sqrt{2\pi}I_v} \exp\left(-\frac{\left(\ln I_v\right)^2}{2\sigma^2} + 2\ln I_v\zeta\right), \tag{79}$$

where $\mu_1' = \mu_1 - \ln I_{v_0}$ and $\mu_2' = \mu_2 - \ln E[I_r|I_v]$. Here, ζ and σ are defined respectively as

$\zeta = \left(\ln I_r + \mu_2'\right)/2\sigma_{d_2}^2 - \mu_1'/2\sigma_{d_1}^2$, and $\sigma = \sqrt{\sigma_{d_1}^2\sigma_{d_2}^2/\left(\sigma_{d_1}^2 + \sigma_{d_2}^2\right)}$.

By replacing (79) in (77), we can rewrite it as

$$f\left(I_r\right) = \vartheta_1 \int_0^{\infty} \frac{\exp\left(-\frac{1}{2\sigma^2}\left(\left(\ln I_v\right)^2 + 2\ln I_v\Upsilon\right)\right)}{I_v\sqrt{2\pi}} dI_v\ , \tag{80}$$

where $\Upsilon = 2\zeta\sigma^2$. By adding and subtracting Υ^2 in exponential argument of (80) and after some mathematical manipulations, we have

$$f\left(I_r\right) = \vartheta_1\sigma \exp\left(\tfrac{1}{2\sigma^2}\Upsilon^2\right) \int_0^{\infty} \frac{\exp\left(-\frac{\left(\ln I_v + \Upsilon\right)^2}{2\sigma^2}\right)}{\sqrt{2\pi}I_v\sigma}\, dI_v. \tag{81}$$

In (81), the term inside the integral is a log-normal distribution with mean Υ and variance σ^2. Recall the fact that $\int_x f(x)\,dx = 1$. Hence by substituting (77) into (80), we can write

$$f(I_r) = \frac{\exp\left(-\frac{(\ln I_r + \mu'_2)^2}{2\sigma_{d_2}^2} - \frac{\mu_1'^2}{2\sigma_{d_1}^2} + \frac{1}{2\sigma^2}\Upsilon^2\right)}{\sqrt{2\pi} I_r \sqrt{\sigma_{d_1}^2 + \sigma_{d_2}^2}}. \tag{82}$$

Finally, by expanding the term inside the exponential function and put it in the form of perfect square binomial, we obtain the final PDF expression given by (11).

APPENDIX B

MAXIMIZATION OF EQ. (30)

In this Appendix, we investigate the maximization of (30). In order to simplify the problem, we investigate two separate cases, namely $SNR_{\mathrm{SR},i} < SNR_{\mathrm{RD},i}$ and $SNR_{\mathrm{SR},i} > SNR_{\mathrm{RD},i}$. Our optimization problem for the first case can be written as

$$\max_{s.t.\ \Delta_1\left(K_{L,i},K_{E,i}\right)\leq\frac{G_{\mathrm{RD}}|H_{\mathrm{RD}}(i)|^2}{G_{\mathrm{SR}}|H_{\mathrm{SR}}(i)|^2}} f_1\left(K_{L,i},K_{E,i}\right)=\left(G_{\mathrm{SR}}|H_{\mathrm{SR}}\left(i\right)|^2\,/\,|H_{\mathrm{SD}}\left(i\right)|^2+1\right)K_{E,i}K_{L,i}^2, \tag{83}$$

where $\Delta_1\left(K_{L,i},K_{E,i}\right)=K_{E,i}K_{L,i}^2/\left[\left(1-K_{E,i}\right)\left(1-K_{L,i}\right)^2\right]$. We form the Lagrange function [43] as

$$L_1\left(K_{L,i},K_{E,i},u\right)=f_1\left(K_{L,i},K_{E,i}\right)+u\left(\frac{G_{\mathrm{RD}}\left|H_{\mathrm{RD}}\left(i\right)\right|^2}{G_{\mathrm{SR}}\left|H_{\mathrm{SR}}\left(i\right)\right|^2}-\Delta_1\left(K_{L,i},K_{E,i}\right)\right), \tag{84}$$

where u is the Lagrange multiplier. Kuhn-Tucker conditions for our problem can be stated as

i) $\frac{\partial L_1}{\partial K_{E,i}}=\left(G_{\mathrm{SR}}|H_{\mathrm{SR}}\left(i\right)|^2\,/\,|H_{\mathrm{SD}}\left(i\right)|^2+1\right)K_{L,i}^2-\frac{uK_{L,i}^2}{\left(1-K_{L,i}\right)^2}\frac{1}{\left(1-K_{E,i}\right)^2}\leq 0$ and $K_{E,i}\frac{\partial L_1}{\partial K_{E,i}}=0$,

ii) $\frac{\partial L_1}{\partial K_{L,i}}=2\left(G_{\mathrm{SR}}|H_{\mathrm{SR}}\left(i\right)|^2\,/\,|H_{\mathrm{SD}}\left(i\right)|^2+1\right)K_{E,i}K_{L,i}-\frac{uK_{E,i}}{\left(1-K_{E,i}\right)}\frac{2K_{L,i}}{\left(1-K_{L,i}\right)^3}\leq 0$ and $K_{L,i}\frac{\partial L_1}{\partial K_{L,i}}=0$,

iii) $u\left(\frac{G_{\mathrm{RD}}|H_{\mathrm{RD}}(i)|^2}{G_{\mathrm{SR}}|H_{\mathrm{SR}}(i)|^2}-\Delta_1\left(K_{L,i},K_{E,i}\right)\right)=0$.

It can be readily checked that $K_{E,i}=0$, $K_{L,i}=0$ and $u=\left(G_{\mathrm{SR}}|H_{\mathrm{SR}}\left(i\right)|^2\,/\,|H_{\mathrm{SD}}\left(i\right)|^2+1\right)\left(1-K_{E,i}\right)^2\left(1-K_{L,i}\right)^2$ satisfy the first condition, i.e., $K_{E,i}\left(\partial L_1/\partial K_{E,i}\right)=0$. Since $K_{E,i}$ and $K_{L,i}$ must be larger than zero, only u is acceptable. We now need to check whether the second condition is satisfied with this u or not. Note that $\partial L_1/\partial K_{L,i}\leq 0$ is satisfied with $u=\left(G_{\mathrm{SR}}|H_{\mathrm{SR}}\left(i\right)|^2\,/\,|H_{\mathrm{SD}}\left(i\right)|^2+1\right)\left(1-K_{E,i}\right)^2\left(1-K_{L,i}\right)^2$ for $K_{E,i}\leq K_{L,i}$. Setting

$K_{L,i}\left(\partial L_1/\partial K_{L,i}\right)$ equal to zero gives us $K_{L,i} = K_{E,i}$. Applying $K_{L,i} = K_{E,i}$ to the third condition, we have

$$K_{L,i}^{\text{opt}} = K_{E,i}^{\text{opt}} = \frac{\sqrt[3]{G_{\text{RD}}\left|H_{\text{RD}}\left(i\right)\right|^2 / \left(G_{\text{SR}}\left|H_{\text{SR}}\left(i\right)\right|^2\right)}}{1+\sqrt[3]{G_{\text{RD}}\left|H_{\text{RD}}\left(i\right)\right|^2 / \left(G_{\text{SR}}\left|H_{\text{SR}}\left(i\right)\right|^2\right)}}. \tag{85}$$

Cooperative system in this case yields an average SNR of $\gamma K_{L,\text{avg}}^2 K_{E,\text{avg}}\left(1+G_{\text{SR}}\right)$ per transmission phase where $K_{L,\text{avg}}$ and $K_{E,\text{avg}}$ are defined in (27). In fact if this summation gives us a value larger than γ (the maximum achievable SNR without cooperation), cooperation brings performance gains. This concludes that we should have the condition $K_{L,\text{avg}}^2 K_{E,\text{avg}}\left(1+G_{\text{SR}}\right) > 1$.

For the second case where $SNR_{\text{SR},i} > SNR_{\text{RD},i}$, our optimization problem is stated as

$$\begin{aligned}\max_{s.t.\ \Delta_2\left(K_{L,i},K_{E,i}\right)\leq\frac{G_{\text{SR}}\left|H_{\text{SR}}(i)\right|^2}{G_{\text{RD}}\left|H_{\text{RD}}(i)\right|^2}} f_2\left(K_{L,i},K_{E,i}\right) &= K_{E,i}K_{L,i}^2 + \left(G_{\text{RD}}\frac{\left|H_{\text{RD}}\left(i\right)\right|^2}{\left|H_{\text{SD}}\left(i\right)\right|^2}\right) \\ &\times\left(1-K_{E,i}\right)\left(1-K_{L,i}\right)^2, \end{aligned}\tag{86}$$

where $\Delta_2\left(K_{L,i},K_{E,i}\right) = \left(1-K_{E,i}\right)\left(1-K_{L,i}\right)^2 / K_{E,i}K_{L,i}^2$. We form the Lagrange function as

$$L_2\left(K_{L,i},K_{E,i},u\right) = f_2\left(K_{L,i},K_{E,i}\right) + u\left(\frac{G_{\text{SR}}\left|H_{\text{SR}}\left(i\right)\right|^2}{G_{\text{RD}}\left|H_{\text{RD}}\left(i\right)\right|^2} - \Delta_2\left(K_{L,i},K_{E,i}\right)\right). \tag{87}$$

Writing Kuhn-Tucker conditions and following the same steps in the first case, the optimization again yields (84). In this case, to test whether the cooperation yields gains or not, we use $K_{L,\text{avg}}^2 K_{E,\text{avg}} + G_{\text{RD}}\left(1-K_{L,\text{avg}}\right)^2\left(1-K_{E,\text{avg}}\right) > 1$.

Bibliography

[1] S. Arnon, J.R.Barry, and G. Karagiannidis, *Advanced optical wireless communication systems*. Cambridge university press, 2012.

[2] S.Arnon, *Visible light communication*. Cambridge University Press, 2015.

[3] Z. Xu and B.M.Sadler, "Ultraviolet communications: potential and state-of-the-art," *IEEE Communications Magazine*, vol. 46, no. 5, pp. 67–73, 2008.

[4] R.J.Drost and B.M.Sadler, "Survey of ultraviolet non-line-of-sight communications," *Semiconductor Science and Technology*, vol. 29, no. 8, p. 084006, 2014.

[5] G. Shaw, A.M.Siegel, and M.L.Nischan, "Demonstration system and applications for compact wireless ultraviolet communications," in *AeroSense 2003*, pp. 241–252, International Society for Optics and Photonics, 2003.

[6] I. C. on Non-Ionizing Radiation Protection *et al.*, "Guidelines on limits of exposure to ultraviolet radiation of wavelengths between 180 nm and 400 nm (incoherent optical radiation)," *Health Physics*, vol. 87, no. 2, pp. 171–186, 2004.

[7] M. Safari and M. Uysal, "Relay-assisted free-space optical communication," *IEEE Transactions on Wireless Communications*, vol. 7, no. 12, pp. 5441–5449, 2008.

[8] R.G.Kizilirmak, O.Narmanlioglu, and M.Uysal, "Relay-assisted OFDM-based visible light communications," *IEEE Transactions on Communications*, vol. 63, no. 10, pp. 3765–3778, 2015.

[9] Q.He, Z.Xu, and B.M.Sadler, "Non-line-of-sight serial relayed link for optical wireless communications," in *Millitary Communicatins Conference*, pp. 1588–1593, IEEE, 2010.

[10] A.Vavoulas, H.G.Sandalidis, and D.Varoutas, "Connectivity issues for ultraviolet UV-C networks," *Journal of Optical Communications and Networking*, vol. 3, no. 3, pp. 199–205, 2011.

[11] A.Vavoulas, H.G.Sandalidis, and D.Varoutas, "Node isolation probability for serial ultraviolet UV-C multi-hop networks," *Journal of Optical Communications and Networking*, vol. 3, no. 9, pp. 750–757, 2011.

[12] C.Gong and Z.Xu, "Non-line of sight optical wireless relaying with the photon counting receiver: A count-and-forward protocol," *IEEE Transactions on Wireless Communications*, vol. 14, no. 1, pp. 376–388, 2015.

[13] Y.Li, L.Wang, Z.Xu, and S.V.Krishnamurthy, "Neighbor discovery for ultraviolet ad hoc networks," *IEEE Journal on Selected Areas in Communications*, vol. 29, no. 10, pp. 2002–2011, 2011.

[14] T.A.Tsiftsis, H.G.Sandalidis, G.K.Karagiannidis, and M.Uysal, "Optical wireless links with spatial diversity over strong atmospheric turbulence channels," *IEEE Transactions on Wireless Communications*, vol. 8, no. 2, pp. 951–957, 2009.

[15] S.M.Navidpour, M.Uysal, and M.Kavehrad, "BER performance of free-space optical transmission with spatial diversity," *IEEE Transactions on wireless communications*, vol. 6, no. 8, pp. 2813–2819, 2007.

[16] M.A.El-Shimy and S.Hranilovic, "Spatial-diversity imaging receivers for non-line-of-sight solar-blind UV communications," *Journal of Lightwave Technology*, vol. 33, no. 11, pp. 2246–2255, 2015.

[17] D.Han, Y.Liu, K.Zhang, P.Luo, and M.Zhang, "Theoretical and experimental research on diversity reception technology in NLOS UV communication system," *Optics express*, vol. 20, no. 14, pp. 15833–15842, 2012.

[18] M.Noshad, M.Brandt-Pearce, and S.G.Wilson, "NLOS UV communications using M-ary spectral-amplitude-coding," *IEEE Transactions on Communications*, vol. 61, no. 4, pp. 1544–1553, 2013.

[19] A.Gupta and M.Brandt-Pearce, "Receiver design for shot noise limited MIMO FSO/UV communication systems," in *2012 IEEE Globecom Workshops*, pp. 1183–1187, 2012.

[20] H.Xiao, Y.Zuo, J.Wu, Y.Li, and J.Lin, "Bit-error-rate performance of non-line-of-sight UV transmission with spatial diversity reception," *Optics letters*, vol. 37, no. 19, pp. 4143–4145, 2012.

[21] M.A.El-Shimy and S.Hranilovic, "Binary-input non-line-of-sight solar-blind uv channels: modeling, capacity and coding," *Journal of Optical Communications and Networking*, vol. 4, no. 12, pp. 1008–1017, 2012.

[22] Q.Gao and G.Chen, "Non-line-of-sight ultraviolet communication based on DHT ACO-OFDM," in *SPIE Optical Engineering+ Applications*, pp. 85170D–85170D, International Society for Optics and Photonics, 2012.

[23] M.R.Luettgen, D.M.Reilly, and J.H.Shapiro, "Non-line-of-sight single-scatter propagation model," *JOSA A*, vol. 8, no. 12, pp. 1964–1972, 1991.

[24] M.A.Elshimy and S.Hranilovic, "Non-line-of-sight single-scatter propagation model for noncoplanar geometries," *JOSA A*, vol. 28, no. 3, pp. 420–428, 2011.

[25] G.Chen, Z.Xu, and B.M.Sadler, "Experimental demonstration of ultraviolet pulse broadening in short-range non-line-of-sight communication channels," *Optics express*, vol. 18, no. 10, pp. 10500–10509, 2010.

[26] H.Ding, G.Chen, A.K.Majumdar, B.M.Sadler, and Z.Xu, "Modeling of non-line-of-sight ultraviolet scattering channels for communication," *IEEE Journal on Selected Areas in Communications*, vol. 27, no. 9, pp. 1535–1544, 2009.

[27] A.Gupta, M.Noshad, and M.Brandt-Pearce, "Nlos uv channel modeling using numerical integration and an approximate closed-form path loss model," in *SPIE Optical Engineering+ Applications*, pp. 851709–851709, International Society for Optics and Photonics, 2012.

[28] Z.Xu, H.Ding, B.M.Sadler, and G.Chen, "Analytical performance study of solar blind non-line-of-sight ultraviolet short-range communication links," *Optics letters*, vol. 33, no. 16, pp. 1860–1862, 2008.

[29] D.L.Hutt and D.H.Tofsted, "Effect of atmospheric turbulence on propagation of ultraviolet radiation," *Optics & Laser Technology*, vol. 32, no. 1, pp. 39–48, 2000.

[30] H.Ding, G.Chen, A.K.Majumdar, B.M.Sadler, and Z.Xu, "Turbulence modeling for non-line-of-sight ultraviolet scattering channels," in *SPIE Defense, Security, and Sensing*, pp. 80380J–80380J, International Society for Optics and Photonics, 2011.

[31] M.H.Ardakani, A.R.Heidarpour, and M.Uysal, "Non-line-of-sight ultraviolet communications over atmospheric turbulence channels," in *4th International Workshop on Optical Wireless Communications (IWOW)*, pp. 55–59, IEEE, 2015.

[32] R.Mesleh, H.Elgala, and H.Haas, "On the performance of different ofdm based optical wireless communication systems," *Journal of Optical Communications and Networking*, vol. 3, no. 8, pp. 620–628, 2011.

[33] O.Amin and M.Uysal, "Optimal bit and power loading for amplify-and-forward cooperative OFDM systems," *IEEE Transactions on Wireless Communications*, vol. 10, no. 3, pp. 772–781, 2011.

[34] T.Wang, A.Cano, G.B.Giannakis, and J.N.Laneman, "High-performance cooperative demodulation with decode-and-forward relays," *IEEE Transactions on Communications*, vol. 55, no. 7, pp. 1427–1438, 2007.

[35] L.Wu, Z.Zhang, J.Dang, and H.Liu, "Adaptive modulation schemes for visible light communications," *Journal of Lightwave Technology*, vol. 33, no. 1, pp. 117–125, 2015.

[36] E.J.Lee and V. W. Chan, "Part 1: Optical communication over the clear turbulent atmospheric channel using diversity," *IEEE Journal on Selected Areas in Communications*, vol. 22, no. 9, pp. 1896–1906, 2004.

[37] M.Safari and M.Uysal, "Cooperative diversity over log-normal fading channels: performance analysis and optimization," *IEEE Transactions on Wireless Communications*, vol. 7, no. 5, pp. 1963–1972, 2008.

[38] J. G. Proakis, "Digital conununications," 2001.

[39] M.Safari and M.Uysal, "Diversity gain analysis of free-space optical communication systems," in *Electrical and Computer Engineering, 2008. CCECE 2008. Canadian Conference on*, pp. 001239–001244, IEEE, 2008.

[40] L.Fenton, "The sum of log-normal probability distributions in scatter transmission systems," *IRE Transactions on Communications Systems*, vol. 8, no. 1, pp. 57–67, 1960.

[41] A.Goldsmith, *Wireless communications*. Cambridge university press, 2005.

[42] M.K.Simon and M.S.Alouini, *Digital communication over fading channels*, vol. 95. John Wiley & Sons, 2005.

[43] M.Luptacik, *Mathematical optimization and economic analysis*. Springer, 2010.

VITA

Maryam Haghighi Ardakani received her B.Sc. degree from the Electrical Engineering department of Isfahan University, Isfahan, Iran in 2013. She is currently pursuing her M.Sc. studies at the department of Electrical and Electronics Engineering, Ozyegin University, Istanbul, Turkey as a research assistant in Communication Theory and Technologies (CT&T) Lab under supervision of Professor Murat Uysal. Her current research mainly focuses on non-line-of-sight ultraviolet communications.